

Continuous mapping of fine particulate matter (PM_{2.5}) air quality in East Asia at daily 6x6 km² resolution by application of a random forest algorithm to 2011-2019 GOCI geostationary satellite data

5 Drew C. Pendergrass¹, Daniel J. Jacob¹, Shixian Zhai¹, Jhoon Kim^{2,3}, Ja-Ho Koo², Seoyoung Lee², Minah Bae⁴, Soontae Kim⁴, and Hong Liao⁵

¹School of Engineering and Applied Sciences, Harvard University, Cambridge, Mass., USA

²Department of Atmospheric Sciences, Yonsei University, Seoul, South Korea

³Particulate Matter Research Institute, Samsung Advanced Institute of Technology (SAIT), Suwon, South Korea

⁴Department of Environmental and Safety Engineering, Ajou University, Suwon., South Korea

10 ⁵Jiangsu Key Laboratory of Atmospheric Environment Monitoring and Pollution Control, Jiangsu Collaborative Innovation Center of Atmospheric Environment and Equipment Technology, School of Environmental Science and Engineering, Nanjing University of Information Science and Technology, Nanjing, Jiangsu, China

Correspondence to: Drew Pendergrass (pendergrass@g.harvard.edu)

Abstract. We use 2011-2019 aerosol optical depth (AOD) observations from the Geostationary Ocean
15 Color Imager (GOCI) instrument over East Asia to infer 24-h daily surface fine particulate matter (PM_{2.5}) concentrations at continuous 6x6 km² resolution over eastern China, South Korea, and Japan. This is done with a random forest (RF) algorithm applied to the gap-filled GOCI AODs and other data, including information encoded in GOCI AOD retrieval failure, and trained with PM_{2.5} observations from the three national networks. The predicted 24-h GOCI PM_{2.5} concentrations for sites entirely
20 withheld from training in a ten-fold crossvalidation procedure correlate highly with network observations ($R^2 = 0.89$) with single-value precision of 26-32% depending on country. Prediction of annual mean values has $R^2 = 0.96$ and single-value precision of 12%. GOCI PM_{2.5} is only moderately successful for diagnosing local exceedances of the National Ambient Air Quality Standard (NAAQS) because these exceedances are typically within the single-value precisions of the RF, and also because
25 of RF smoothing of extreme PM_{2.5} concentrations. The area-weighted and population-weighted trends of GOCI PM_{2.5} concentrations for eastern China, South Korea, and Japan show steady 2015-2019 declines consistent with surface networks, but the surface networks in eastern China and South Korea underestimate population exposure. Further examination of GOCI PM_{2.5} fields for South Korea identifies hotspots where surface network sites were initially lacking and shows 2015-2019 PM_{2.5}
30 decreases across the country except for flat concentrations in the Seoul metropolitan area. Inspection of monthly PM_{2.5} time series in Beijing, Seoul, and Tokyo shows that the RF algorithm successfully captures observed seasonal variations of PM_{2.5} even though AOD and PM_{2.5} often have opposite seasonalities. Application of the RF algorithm to urban pollution episodes in Seoul and Beijing demonstrates high skill in reproducing the observed day-to-day variations in air quality as well as
35 spatial patterns on the 6 km scale. Comparison to a CMAQ simulation for the Korean peninsula demonstrates the value of the continuous GOCI PM_{2.5} fields for testing air quality models, including over North Korea where they offer a unique resource.

1. Introduction

40 Exposure to outdoor fine particulate matter (PM_{2.5}, less than 2.5 μm in diameter) is a global public health issue, accounting for 8.9 million deaths in 2015 [Burnett et al., 2018]. Beyond mortality, short-term exposure to elevated PM_{2.5} levels is associated with numerous adverse health outcomes including increased hospital admissions for respiratory and cardiovascular issues [Dominici et al., 2006; Wei et al., 2019]. Long-term exposure is associated with neurodegenerative diseases such as dementia, Alzheimer's disease, and Parkinson's disease [Kioumourtzoglou et al., 2016]. High spatio-temporal
45 monitoring of PM_{2.5} concentrations to inform population exposure is important for both air quality regulation and epidemiological studies. Ground monitors can provide highly accurate measurements but have limited spatial coverage. Here we show how geostationary satellite observations of aerosol optical depth (AOD) over East Asia from the Geostationary Ocean Color Imager (GOCI) can be used with a random forest (RF) machine learning (ML) algorithm to provide continuous long-term reliable mapping
50 of 24-h PM_{2.5} at 6x6 km² spatial resolution.

The potential of satellites for high-resolution monitoring of PM_{2.5} has long been recognized in the public health community [Liu et al., 2004; van Donkelaar et al., 2006]. Satellites retrieve AOD by backscatter of solar radiation. The MODIS sensors launched in 1999 on the NASA Terra and Aqua
55 satellites have been the main source of AOD data, with global coverage twice a day at up to 1 km resolution [Remer et al., 2005, 2013; Lyapustin et al., 2018]. Early approaches to relate AOD observations to surface PM_{2.5} used chemical transport models (CTMs) to estimate local PM_{2.5}/AOD ratios [Liu et al., 2004; van Donkelaar et al., 2006], with more recent studies adding ancillary satellite data on the vertical distribution of aerosol extinction [Geng et al., 2015; van Donkelaar et al., 2016; van Donkelaar et al., 2019]. Other approaches have used PM_{2.5} network data to infer PM_{2.5}/AOD ratios
60 [Wang and Christopher, 2003], with statistical models based on meteorological and land-use predictor variables to enable spatial extrapolation [Gupta and Christopher, 2009; Liu et al., 2009; Kloog et al., 2012; 2014].

More recently, non-parametric machine learning models have been developed to predict PM_{2.5} from satellite AOD observations including neural networks [Li et al., 2017; Zang et al., 2019] and
65 RFs, including approaches that fuse both [Di et al., 2019]. RF has been applied to MODIS AOD to produce high-resolution daily PM_{2.5} products for the US [Hu et al., 2017] and China [Guo et al., 2021]. Others have used RF and satellite AODs to produce monthly PM_{2.5} data over the North China Plain [Huang et al., 2018], as well as daily PM_{2.5} data in California [Geng et al., 2020] and Cincinnati, Ohio [Brokamp et al., 2018].

70 Geostationary satellites are now dramatically increasing the capability for mapping of PM_{2.5} from space. The GOCI instrument launched in 2010 by the Korea Aerospace Research Institute (KARI) observes AOD eight times daily at 0.5x0.5 km² pixel resolution over eastern China, the Korean peninsula, and Japan [Choi et al., 2018]. The fine-pixel hourly information is intrinsically valuable and also facilitates cloud clearing [Remer et al., 2012]. GOCI AOD data aggregated to 6x6 km² resolution
75 have been used to estimate PM_{2.5} in regional studies for the Yangtze River Delta [She et al., 2020] and eastern China [Xu et al., 2015]. Park et al. [2019] find that PM_{2.5} can be inferred over the Korean peninsula with greater accuracy using GOCI AOD than sparser MODIS data. AOD products from the Advanced Himawari Imager (AHI) onboard the Himawari-8 and -9 geostationary meteorological

80 satellites over East Asia have also been used to infer surface $PM_{2.5}$ [Wang *et al.*, 2017; Chen *et al.*, 2019].

AOD cannot be observed under cloudy conditions, and AOD retrievals from satellites can also fail for other reasons including snow surfaces. Different methods have been used to fill the data gaps and produce continuous data sets. Some studies use CTM AODs when satellite data are missing [Hu *et al.*, 2017; Stafoggia *et al.*, 2019]. Kianian *et al.* [2021] used a statistical interpolation algorithm
85 combining RF with the lattice kriging method to infer missing AOD over the US, while Di *et al.*, [2019] used a RF trained on gap-free covariates to fill in the gaps for MODIS AOD. Yet others first estimate $PM_{2.5}$ using available AOD observations, then infer missing $PM_{2.5}$ estimates using a separate gap-filling model [Kloog *et al.*, 2014; She *et al.*, 2020]. Brokamp *et al.* [2018] show that AOD missingness is itself
90 predictive of $PM_{2.5}$, an insight we leverage in this work.

Here we apply a RF algorithm to 2011-2019 GOCI AOD data to construct a continuous dataset of 24-h $PM_{2.5}$ concentrations at 6×6 km² resolution for eastern China, South Korea, and Japan trained with surface network data. This is a larger spatial domain than has been attempted in previous studies. We ensure continuity by using gap-filled AOD, calculated by blending a CTM simulation with statistical interpolation, along with a parameter characterizing the length scale of the interpolation as
95 inputs to the RF algorithm. This strategy maximizes training set size and allows the RF to determine a strategy to handle information encoded by retrieval failure. The resulting gap-filled product predicts $PM_{2.5}$ with comparable skill when AOD observations are absent as when they are available. We characterize the error in the RF-produced GOCI $PM_{2.5}$ dataset for both 24-h and annual concentrations and demonstrate the ability of the dataset to capture spatial and day-to-day variability on urban scales.
100 We exploit the continuity of the dataset to determine trends of $PM_{2.5}$ air quality in East Asia over the past half decade.

2 Data and methods

2.1 Datasets

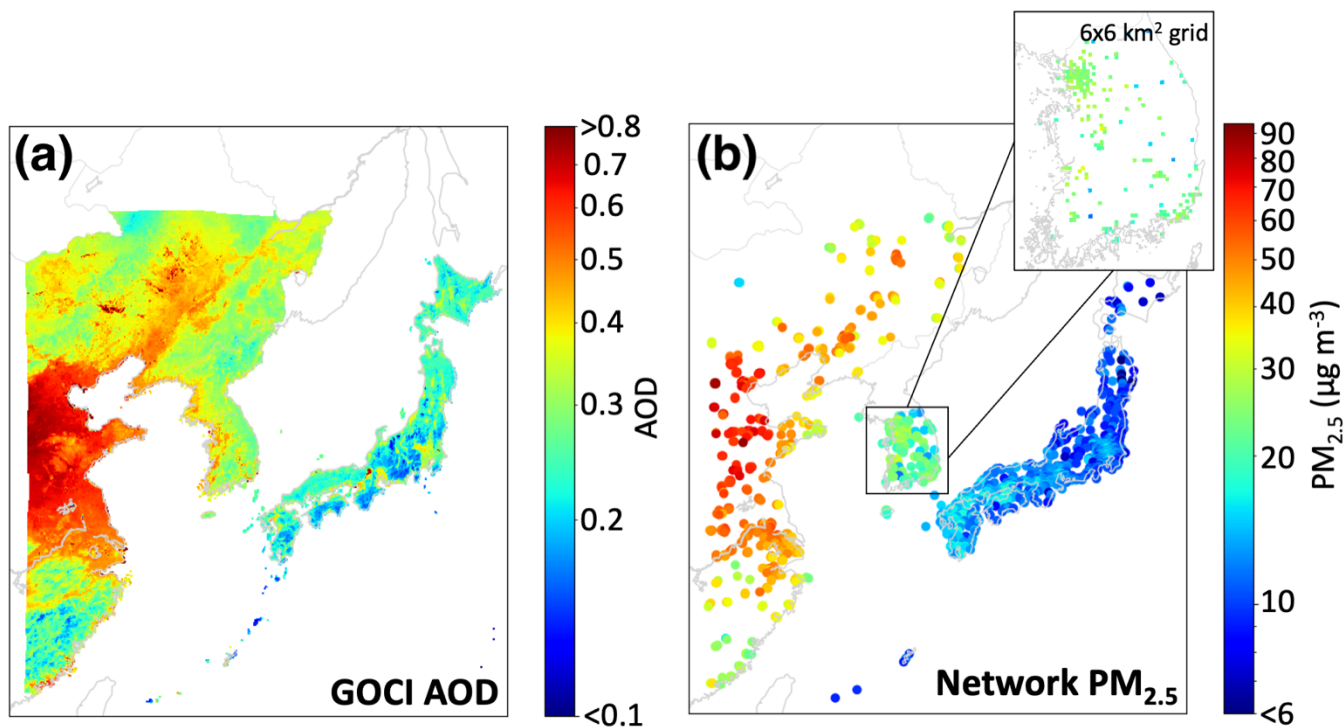
GOCI AODs. GOCI is onboard the Korean Communication, Ocean, and Meteorological Satellite (COMS) that was launched by KARI in June 2010 [Choi *et al.*, 2012; Choi *et al.*, 2016]. The first
105 ocean color imager placed in geostationary orbit, GOCI covers a $2,500 \times 2,500$ km² domain centered on the Korean peninsula at 36°N and 130°E with 0.5×0.5 km² pixels observed every hour from 00:30 to 07:30 UTC. AOD at 550 nm over land is retrieved using the GOCI Yonsei aerosol retrieval (YAER) V2 algorithm at an aggregated 6×6 km² spatial resolution and 1 h temporal resolution [Choi *et al.*, 2018].
110 Aggregation filters out pixels affected by sunglint or clouds, as well as the darkest 20% and brightest 40% pixels within the 6×6 km² scene [Choi *et al.*, 2018]. We further aggregate the hourly AOD measurements of AOD into a daily mean for use in the RF.

Validation of the GOCI YAER V2 AOD with surface measurements from the AERONET surface network shows high correlation ($R = 0.91$), a root mean squared error (RMSE) of 0.16, and a
115 mean bias (MB) of 0.01 with no significant spatial variation across East Asia [Choi *et al.*, 2018]. GOCI YAER V2 also reports a Fine Mode Fraction (FMF) and a Multiple Prognostic Expected Error (MPEE) for the AOD but we find that they are not useful in our RF, as discussed later. For comparison, we also

120 calculate a RF trained on the GOCI-AHI fusion AOD product of *Lim et. al.* [2021]. The Advanced
Himawari Imager (AHI) instruments onboard the Himawari-8 and -9 geostationary meteorological
satellites were launched in October 2014 and November 2016, respectively. AHI has a larger field of
view than GOCI but a shorter record.

125 *PM_{2.5} network data.* We use hourly PM_{2.5} data from operational air quality networks in eastern
China, South Korea, and Japan, and average them over 24 hours and over the 6x6 km² GOCI AOD grid
to define targets for the RF algorithm. Data for eastern China are from the National Environmental
Monitoring Center (<https://quotsoft.net/air/>) including 443 sites within the GOCI observing domain
starting in May 2014 and increasing to 596 sites by 2019. Following *Zhai et. al.* [2019] we remove
values with more than 24 consecutive repeats in the hourly timeseries as likely in error. Data for South
Korea are from the AirKorea surface network of 123 sites (<https://www.airkorea.or.kr/>) starting in
130 January 2015 and increasing to 298 sites by 2019. Data for Japan are from 1054 sites reported by the
Japanese National Institute for Environmental Studies (NIES) for 2011-2017
(https://www.nies.go.jp/igreen/tj_down.html) and by the real-time Atmospheric Environmental
Regional Observation System (AEROS) portal for 2018-2019 (Soramame;
<http://soramame.taiki.go.jp/Download.php>).

135



140 Figure 1: Mean aerosol optical depth (AOD) and surface network PM_{2.5} concentrations over the Geostationary Ocean Color Imager (GOCI) viewing domain, 2011-2019. Panel (a) shows mean GOCI AOD data on the 6x6 km² grid. Panel (b) shows the mean surface network PM_{2.5} data for eastern China (starting in May 2014), South Korea (starting in January 2015), and Japan, using large data symbols for visibility. Zoomed inset for South Korea shows the surface network observations with symbols corresponding to the 6x6 km² grid of the GOCI data. Log scale is used for colorbar.

Meteorological and geographical predictor variables. We use hourly meteorological data from the ERA5 global reanalysis, with resolution of $30 \times 30 \text{ km}^2$ [Hersbach et al., 2020], as input predictor variables for the RF algorithm. For this purpose we aggregate the data to 24-h averages and allocate them to $6 \times 6 \text{ km}^2$ GOCI grid cells by bilinear interpolation. We consider boundary layer height, 2-m air temperature and relative humidity (RH), 10-m meridional and zonal winds, and sea level pressure as potential meteorological predictor variables. We also include latitude, year, day of year (1-366), and nation category (eastern China, South Korea, or Japan) as geographical predictor variables. We considered 2015 population density [CIESIN, 2018] as a potential predictor variable but found that it was not useful as discussed in section 3.2.

Figure 1 shows the mean distributions of GOCI AOD and surface network $\text{PM}_{2.5}$ for 2011-2019 or for the more limited durations of their records (2014-2019 for eastern China $\text{PM}_{2.5}$, 2015-2019 for South Korea $\text{PM}_{2.5}$). The $\text{PM}_{2.5}$ networks are extensive but coverage is nevertheless sparse and often limited to large urban areas, as illustrated by the zoomed inset for South Korea. We find that only 1.0% of GOCI $6 \times 6 \text{ km}^2$ grid cells have $\text{PM}_{2.5}$ observations in eastern China, 7.4% in South Korea, and 7.9% in Japan. This geographic limitation in the $\text{PM}_{2.5}$ networks emphasizes the value of continuous coverage from the AOD data.

2.2 AOD gap-filling

% of days with GOCI AOD observations, 2011-2019

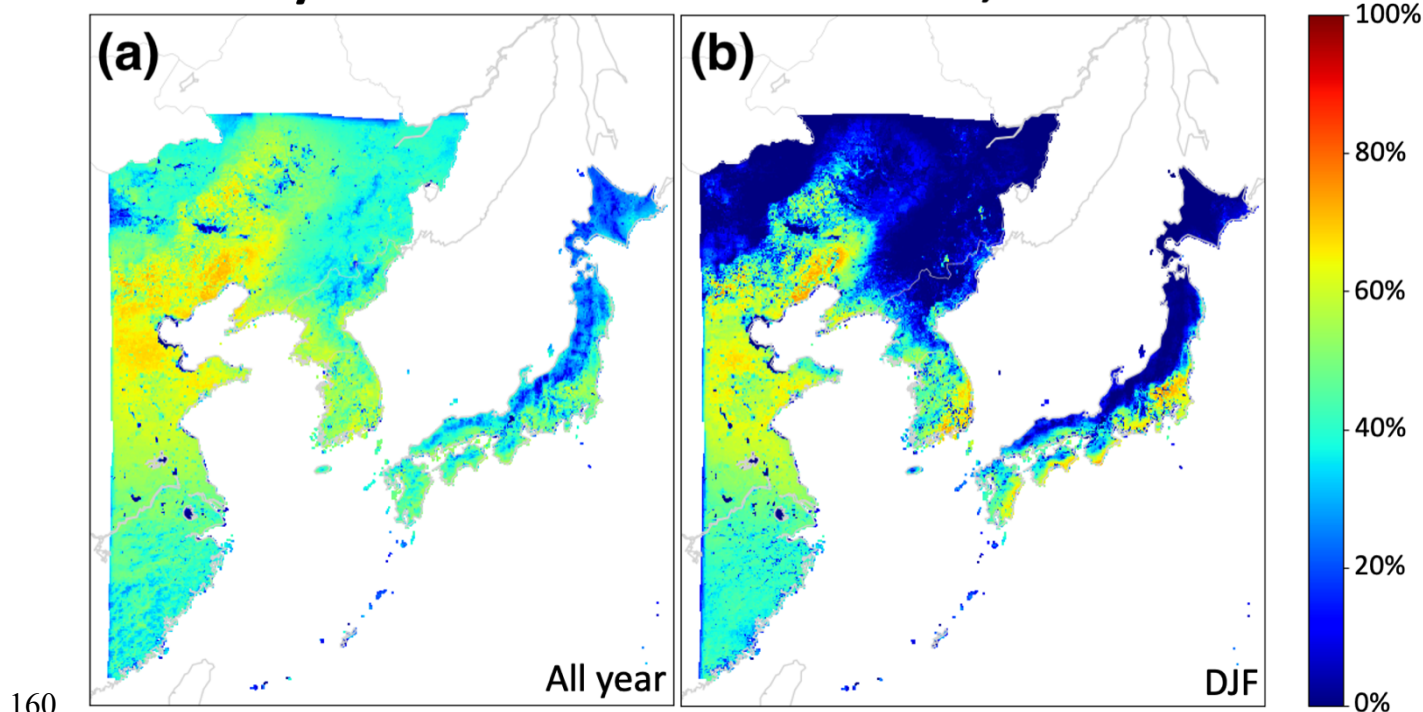


Figure 2: Percentage of days in 2011-2019 with at least one successful hourly retrieval of AOD on the $6 \times 6 \text{ km}^2$ grid. Panel (a) shows year-round statistics while panel (b) shows winter months (DJF) only.

Figure 2 shows the percentage of days with at least one successful hourly GOCI AOD retrieval on the 6x6 km² retrieval grid. There are substantial gaps in the record, mostly reflecting clouds and also snow cover in winter [Choi *et al.*, 2018]. We seek to fill in these gaps to produce a continuous daily data set while accounting for the associated errors and leveraging information implicitly encoded in retrieval failure. We fuse two strategies according to the availability of nearby AOD retrievals: an inverse distance weighted (IDW) interpolation AOD_{IDW} of nearby retrievals [Shepard, 1968] and a bias-corrected monthly AOD_{GC} from the GEOS-Chem CTM:

$$\text{AOD} = \alpha \text{AOD}_{\text{IDW}} + (1 - \alpha)\text{AOD}_{\text{GC}} \quad (1)$$

where α is a weighting factor that depends on the distance from nearest retrievals. GEOS-Chem is a widely used CTM for inferring PM_{2.5} from satellite AOD data [Liu *et al.*, 2004; van Donkelaar *et al.*, 2006; 2016; 2019; Geng *et al.*, 2015]. Here we use scaled monthly mean GEOS-Chem AODs from a simulation by Zhai *et al.* [2021] for 2016 in East Asia with 0.5°x 0.625° resolution, bias-corrected to the annual mean GOCI AODs on the 6x6 km² grid. In this way we obtain a spatial distribution of monthly mean AOD_{GC} values for 2011-2019 for use in equation (1).

We calculate the weighting factors α used in Equation (1) via the Gaspari-Cohn function, a fifth-order piecewise polynomial with a radial argument r [Gaspari and Cohn, 1999]. The Gaspari-Cohn function resembles a Gaussian distribution but with compact support, taking on a maximum value of 1 for $r = 0$ and a minimum value of 0 for $r \geq 2$. We define $r = l/c$ for a given 6x6 km² grid cell and day to be the distance l from the midpoint of the grid cell to that of the nearest observed grid cell, normalized by a spatial correlation length scale c determined from available AOD observations in and around that grid cell. We find that the value of c ranges from 110 km to 170 km over our domain.

185 2.3 Random forest algorithm

Table 1 lists the predictor variables included in the RF to infer 24-h PM_{2.5} as dependent variable. RF is an ensemble machine learning method where many individual decision trees are fit to the training data and vote on an output value, with the average value taken as best estimate [Breiman, 2001].

Table 1. Random Forest predictor variables for 24-h PM_{2.5}^a

GOCI gap-filled AOD observations ^b
8-h average AOD at 550 nm wavelength
α from Equation 1
Meteorology ^c
Boundary layer height (m)
10-m meridional wind (m s ⁻¹)
10-m zonal wind (m s ⁻¹)
2-m temperature (K)
2-m relative humidity ^d (%)
Sea-level pressure (Pa)
Metadata

Country dummy variables^c

Latitude

Day of year

Year

190 ^aThe RF algorithm predicts continuous 24-h PM_{2.5} on a 6x6 km² grid for eastern China, South Korea, and Japan after training with PM_{2.5} surface network data.

^b8-hr average 550 nm AODs on the 6x6 km² grid retrieved with the YAER v2 algorithm [Choi et al., 2018]

^cECMWF ERA5 fields [Hersbach et al., 2020] at 30x30 km² spatial resolution and hourly temporal resolution, interpolated bilinearly to the GOCI grid and averaged over 24 hours.

195 ^dEstimated from temperature and dewpoint using the August-Roche-Magnus approximation [Alduchov and Eskridge, 1996].

^eThree variables that, for each of eastern China, South Korea, and Japan, has value 1 if a grid cell is within those national borders and 0 otherwise.

Decision trees are fit recursively to the predictor variable. Suppose we have a collection of N data
200 elements $i \in [1, N]$, denoted x_i , each composed of m predictor variables ($x_i \in \mathbb{R}^m$), and a corresponding
list of N labels y_i that we would like to learn. In our case y_i denotes the observed PM_{2.5} concentrations
from the surface networks averaged on the 6x6 km² grid, and N denotes the number of these
observations. The algorithm works by splitting the data into left and right subsets L and R at an
optimum split point determined from the predictor variables in x_i [Pedregosa et al., 2011]. The
205 optimum split point is defined as the one that minimizes the impurity G ,

$$G(L, R) = \beta \cdot \text{MSE}(L) + (1 - \beta) \cdot \text{MSE}(R) \quad (2)$$

where β represents the fraction of data in the subset L and MSE represents the mean squared error of
each of the subsets,

$$\text{MSE}(X) = \frac{1}{n} \sum_i (y_i - \bar{y})^2 \quad (3)$$

where \bar{y} is the mean of the target labels within a given subset X and n is the number of elements in that
subset. From there the same algorithm is recursively applied to the left and right subsets L and R until
210 the tree is grown. We follow the advice of *Hastie et al.* [2009] and grow trees until the data are fully
classified (each leaf contains only one value).

Due to the recursive training structure, decision trees are sensitive to the data on which they are
trained, because a change in one split point changes the composition of all its child nodes. Individual
decision trees thus have high error variance but no inherent bias. It follows that averaging many
215 individual and uncorrelated trees should yield a low variance, low bias prediction. We construct 200
trees in parallel and reduce correlation between them through a bagging procedure: for each of the 200
decision trees in the RF, sample the input data with replacement to form a new dataset of the same
dimensions and then grow a decision tree from this bootstrapped data [Breiman, 2001]. Because of the
high input sensitivity, a wide variety of decorrelated trees are grown. The predictions of each individual
220 tree are averaged to yield the prediction of the RF. We fit our RF using the RandomForestRegression
class in the Python module Scikit-learn [Pedregosa et al., 2011]. We attempted to further decorrelate
trees by following *Breiman* [2001] and calculating split points of each individual tree using only a
random subset of the m predictor variables; however, a sensitivity test we performed showed only minor
differences with the base case and therefore we follow *Guerts et al.* [2006] in considering all predictor
225 variables in the training process.

We evaluate how the RF generalizes to predictions for the full 6x6 km² domain via a 10-fold crossvalidation. For each fold of the crossvalidation, we leave out a randomly selected 10% of PM_{2.5} network sites (averaged on the 6x6 km² grid if needed) from each country. These 10% represent the test set; because we perform the validation ten times, each grid cell is in the test set exactly once. We
 230 compare predicted PM_{2.5} to withheld observed PM_{2.5} using four metrics: root mean square error (RMSE); the RMSE divided by mean observed PM_{2.5} (relative RMSE, or RRMSE); the coefficient of variation (R²); and the mean bias computed by averaging the difference between predicted and observed PM_{2.5} (MB).

An outcome of interest is the ability of our predictions to capture exceedances of National
 235 Ambient Air Quality Standards (NAAQS). We categorize each prediction within the test sets into one of four classes: true positives (TP) where both predicted and observed PM_{2.5} exceed the NAAQS threshold; true negatives (TN) where neither exceed the threshold; false positives (FP) where an exceedance is predicted but not observed; and false negatives (FN) where an exceedance is observed but not predicted [Brasseur and Jacob, 2017; Cusworth et. al., 2018]. We use these classes to compute
 240 three overall prediction grades. The first, percent of detection (POD), gives the fraction of observed exceedances that were successfully predicted:

$$\text{POD} = \frac{\Sigma \text{TP}}{\Sigma \text{TP} + \Sigma \text{FN}} \quad (4)$$

The second, false alarm ratio (FAR), gives the fraction of predicted exceedances that did not occur:
 245

$$\text{FAR} = \frac{\Sigma \text{FP}}{\Sigma \text{TP} + \Sigma \text{FP}} \quad (5)$$

The third, equitable threat score (ETS), compares how well the prediction does relative to random chance:

$$\text{ETS} = \frac{\Sigma \text{TP} - \beta}{\Sigma \text{TP} + \Sigma \text{FP} + \Sigma \text{FN} - \beta} \quad (6)$$

250 where β is the number of true positives obtained by random chance,

$$\beta = \frac{(\Sigma \text{TP} + \Sigma \text{FP}) \cdot (\Sigma \text{TP} + \Sigma \text{FN})}{\Sigma \text{TP} + \Sigma \text{TN} + \Sigma \text{FP} + \Sigma \text{FN}} \quad (7)$$

255 ETS is 1 for perfect prediction skill and 0 for no better or worse than chance.

Predictor variable selection is an important task in implementing a RF, as the addition of non-informative variables can decrease performance. Unlike linear regression which can naturally ignore unhelpful predictors, irrelevant data can by chance aid in minimizing impurity G at some stage in the

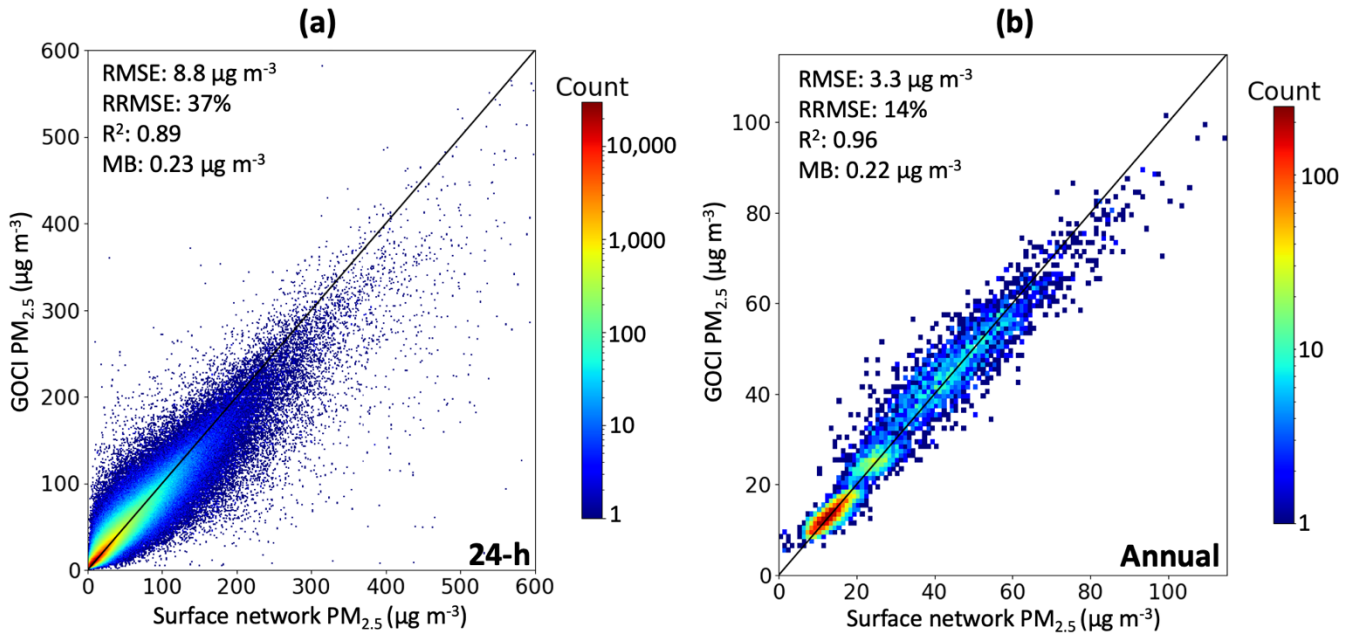
260 optimization process making all subsequent splits suboptimal. The six meteorological variables given in
Table 1 are standard in AOD/PM_{2.5} prediction [e.g. *Kloog et al.*, 2014; *Li et al.*, 2017], while the four
spatio-temporal variables (location dummies, latitude, year, and day of year) and the retrieval gapfilling
parameter α proved to be informative in sensitivity tests. In addition to the predictor variables in **Table**
265 **1**, we considered as additional variables the population density, the GOCI fine mode fraction (FMF),
and the GOCI multiple prognostic expected error (MPEE), but we found that they worsened accuracy of
the fit and so we did not retain them. Because population density worsened the fit we did not include
other spatially varying but temporally fixed land-use variables such as road data, elevation, or
emissions. We also compared RFs trained on GOCI AOD and on GOCI-AHI fused AOD and found no
significant difference in the fitting of PM_{2.5}. We therefore use the GOCI AOD product because of its
270 longer record.

3 Results and discussion

3.1 Accuracy and precision of RF predictions

Figure 3 shows scatterplots, color-coded by count, comparing surface observations of 24-h and annual
mean PM_{2.5} to the predicted GOCI PM_{2.5} values in grid cells whose records are entirely withheld from
275 training in the crossvalidation procedure. GOCI PM_{2.5} values for the annual mean are obtained by
averaging the 24-h predictions. **Table 2** gives comprehensive GOCI PM_{2.5} evaluation statistics for East
Asia and for each country. The 24-h predictions for East Asia have a negligible mean bias of 0.23 $\mu\text{g m}^{-3}$
(annual, 0.22 $\mu\text{g m}^{-3}$), though the RF underpredicts PM_{2.5} at the high tail of the distribution; we will
return to that issue later in the context of NAAQS exceedances. Root mean square error (RMSE)
280 between observed and predicted 24-h PM_{2.5} is 8.8 $\mu\text{g m}^{-3}$ (annual, 3.3 $\mu\text{g m}^{-3}$) corresponding to a
relative RMSE (RRMSE) of 37% (annual, 14%), as defined in section 2.3. The prediction captures 89%
of the observed 24-h variance ($R^2 = 0.89$) and 96% of annual ($R^2 = 0.96$). These results compare
favorably to previous reconstructions of PM_{2.5} from satellite AOD data. For example, a 1-km 2000-
2015 continental US product and 3-km 2015-2016 east China product have crossvalidation R^2 of 0.86
285 and 0.87 respectively for daily PM_{2.5} [*Di et al.*, 2019; *Hu et al.*, 2019], while a global 0.01° 1998–2018
product and a 0.1° degree 2000-2016 product for China have crossvalidated R^2 of 0.90-0.92 and 0.77
respectively for annual PM_{2.5} [*Hammer et al.*, 2020; *Xue et al.*, 2019]. R^2 for annual mean PM_{2.5} in
South Korea is relatively low (0.41), which can be explained by the weak dynamic range of observed
annual PM_{2.5} in the country (**Figure 1**), as will be discussed later in this section.

290 Our gap-filling strategy does not introduce bias for days without GOCI observations (and with
AOD inferred instead from equation (1)). **Figure S1** shows that surface network PM_{2.5} has distinct
distributions on days where AOD retrieval fails as compared to when AOD retrieval succeeds, a pattern
successfully reproduced by GOCI PM_{2.5}. **Table 2** shows that the mean bias statistic on days where AOD
retrieval fails is similar to the whole population. This suggests that the RF algorithm is able to
295 successfully exploit the information encoded in AOD missingness in making a PM_{2.5} prediction, a
phenomenon also noted by *Brokamp et al.* [2018].



300 Figure 3: Ability of the random forest algorithm to predict 24-h (panel a) and annual mean PM_{2.5} (panel b) in East Asia. Scatterplots depict
 305 the relationship between GOCI and surface network PM_{2.5} at grid cells withheld from training in the crossvalidation. The plots are two-
 dimensional histograms where pixel color corresponds to the count of observation/prediction correspondences within the corresponding bin
 on a logged scale. The identity line is plotted in black. For annual mean PM_{2.5}, grid cells with fewer than 80% of PM_{2.5} observation days in
 a given year are removed to avoid biasing the average. For panel (a), 0.002% of the data are not shown as they exceed the plot range; all
 data are shown in panel (b).

Table 2. Error statistics for fitting of PM_{2.5} data by the RF algorithm^a

	RMSE ($\mu\text{g m}^{-3}$)	RRMSE	R ²	MB ($\mu\text{g m}^{-3}$)	MBnr ($\mu\text{g m}^{-3}$)
24-h PM _{2.5}					
Overall	8.8	37%	0.89	0.23	0.23
Eastern China	15	32%	0.85	0.49	0.53
South Korea	6.4	26%	0.82	0.16	0.10
Japan	3.6	27%	0.79	0.12	0.13
Annual PM _{2.5}					
Overall	3.3	14%	0.96	0.22	
Eastern China	5.6	12%	0.86	0.53	
South Korea	2.9	12%	0.41	0.24	
Japan	1.6	12%	0.70	0.094	

^aComparison statistics between GOCI and surface network PM_{2.5} are for the grid cells in each of eastern China, South Korea, and Japan completely withheld from the RF training process in the crossvalidation procedure. Statistics shown are for root-mean-square error (RMSE), relative RMSE (RRMSE), coefficient of variation (R²), and mean bias (MB), and mean bias on days where AOD retrieval fails (MBnr).

310 One potential application of PM_{2.5} monitoring from space would be to diagnose exceedances of national ambient air quality standards (NAAQS) at locations without network sites. **Table 3** shows the

315 NAAQS for 24-h and annual PM_{2.5} for the three countries and the ability of GOCI PM_{2.5} to diagnose
 NAAQS exceedances in grid cells excluded from the training process in the crossvalidation procedure.
 24-h exceedances correspond to the high tails of the distributions but annual exceedances are much
 more widespread. The POD column shows percent of true positives successfully detected, while the
 FAR shows the rate of false positives (defined in section 2.3). POD for 24-h exceedances ranges from
 47%-78% by country (FAR: 16%-21%). PODs are higher for annual exceedances but that reflects the
 higher observed frequency of these exceedances. The ETS values ranging from 0.43-0.63 indicate that
 the model captures exceedances with much better skill than random guessing.

320

Table 3. Ability of the RF algorithm to diagnose exceedances of air quality standards^a

	NAAQS ($\mu\text{g m}^{-3}$) ^b	Exceedance frequency ^c		POD ^d	FAR ^e	ETS ^f
		Observed	RF			
24-h PM _{2.5}						
Eastern China	75	16%	15%	78%	16%	0.63
South Korea (old NAAQS)	50	5.9%	4.2%	57%	21%	0.47
South Korea (new NAAQS)	35	19%	17%	73%	20%	0.55
Japan	35	1.6%	0.91%	47%	17%	0.43
Annual PM _{2.5}						
Eastern China	35	77%	83%	97%	9.2%	0.54
South Korea (old NAAQS)	25	40%	44%	67%	39%	0.23
South Korea (new NAAQS)	15	100%	100%	100%	0%	NA
Japan	15	24%	20%	68%	20%	0.49

^a Calculated using sites withheld from training in the crossvalidation procedure.

^b National Ambient Air Quality Standards, specific to each country. We show results for the class 2 NAAQS in eastern China and for both pre-2018 ('old') and post-2018 ('new') NAAQS for South Korea because all observed grid cells exceed the new annual NAAQS of 15 $\mu\text{g m}^{-3}$.

325 ^c Percentage of site-days (24-h standard) or site years (annual standard) exceeding the NAAQS.

^d Percent of detection (POD) defined as the percentage of exceedances successfully detected.

^e False alarm ratio (FAR) defined as the percentage of predicted exceedances that did not occur.

^f Equitable threat score (ETS) defined as the ability of the RF to predict exceedances beyond random chance.

330

The main difficulty for GOCI PM_{2.5} to predict NAAQS exceedances is that many of those
 exceedances fall within the precision of individual predictions. This is illustrated in **Figure 4** with the
 cumulative probability density function (pdf) of the 24-h and annual mean PM_{2.5} concentrations in
 eastern China, South Korea, and Japan, representing the same withheld data from the crossvalidation as
 in **Tables 2** and **3**. The 24-h RRMSE of 26-32% depending on country (**Table 2**) is shown as the grey
 envelope and is relatively flat across the distribution. Prediction of NAAQS exceedances within that
 uncertainty envelope is limited by the precision of the algorithm. All of the 24-h exceedances in Japan
 are within that envelope, as are most of the exceedances in eastern China and Korea. China has the
 largest fraction of exceedances beyond the RRMSE of the GOCI PM_{2.5} and therefore the best prediction
 success. An additional though smaller cause of bias is that GOCI PM_{2.5} underestimates the high tail of
 the pdf, as is apparent in **Figure 4**, which explains in particular why we achieve a better FAR than POD
 for 24-h PM_{2.5} in South Korea and Japan. Our worst NAAQS prediction performance is for annual
 PM_{2.5} in South Korea for the old 25 $\mu\text{g m}^{-3}$ standard, because most of the distribution is within the

340

RRMSE envelope. Additionally, the already small dynamic range of surface network annual $\text{PM}_{2.5}$ (black dots) is underestimated by the GOCI $\text{PM}_{2.5}$ (blue dots). These culminate in a GOCI $\text{PM}_{2.5}$ estimate with good RMSE but low R^2 .

345

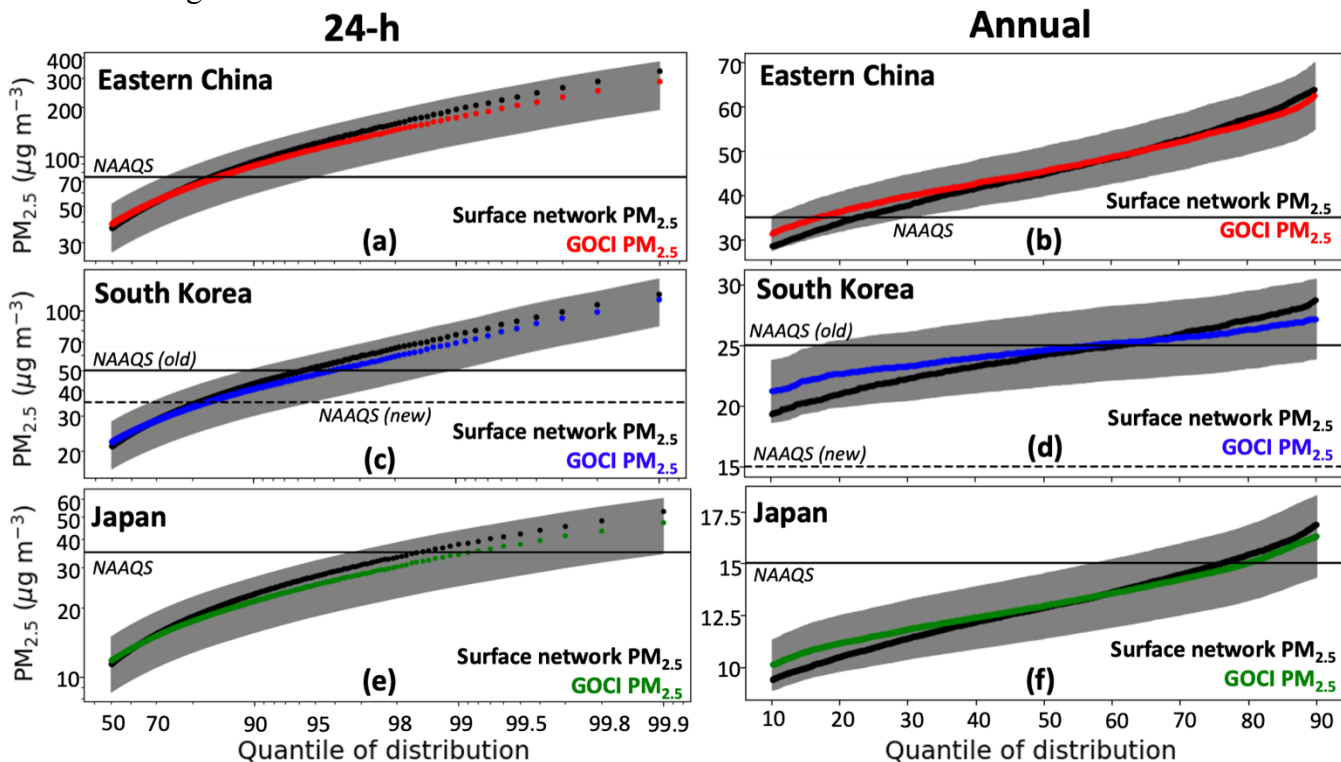


Figure 4: Cumulative probability density functions (pdfs) of 24-h and annual mean $\text{PM}_{2.5}$ concentrations in Eastern China, South Korea, and Japan. Surface network $\text{PM}_{2.5}$ (black) is compared to GOCI $\text{PM}_{2.5}$ (colored) taken from the crossvalidation. The grey envelope represents the relative root mean square error (RRMSE) of the RF algorithm as given in Table 2, measuring the predictive capability of the algorithm for individual events. The NAAQS for each country is shown as the horizontal line, with both the pre-2018 and post-2018 NAAQS shown for South Korea. Left panel scales are log-log while right-panel scales are linear. y-axis scales vary for the different countries.

350

We experimented with several modifications to the RF algorithm to improve prediction of NAAQS exceedances but with no success. These tests included training separate RFs for each of the three countries; training annual $\text{PM}_{2.5}$ predictions on annual (rather than 24-h) $\text{PM}_{2.5}$ data; directly predicting NAAQS exceedances by setting the learned label to be true if a day (year) is above the 24-h (annual) NAAQS for a given country; and applying different weights to the data so that the high tail is oversampled in the training process. None of these tests yielded significant improvements. Smoothing of the tails in RFs is a well-recognized problem [Zhang and Lu, 2012]. Following Zhang and Lu [2012] we attempted to train RFs to predict and correct the residuals but found this to be ineffective. Part of this tail smoothing could also result from the underlying GOCI AOD land product, which has a negative bias (-0.02) for high AODs and a positive bias (+0.02) for low AODs [Choi et. al., 2018].

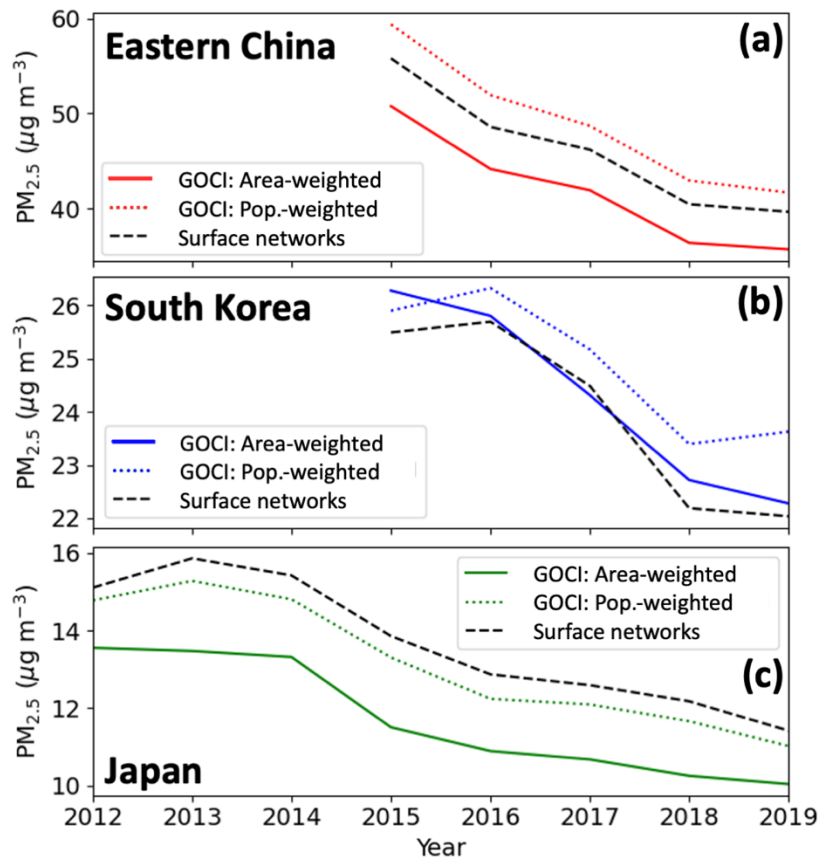
355

360

3.2 PM_{2.5} temporal trends and spatial distributions

365 **Figure 5** shows long-term trends of annual PM_{2.5} for each country, as measured by the PM_{2.5} surface network and as inferred in the GOCI PM_{2.5} for both areal and population-weighted means. We do not include GOCI PM_{2.5} for years before the networks became available (and hence when the RF could be trained) because of concern over extrapolation bias. The PM_{2.5} networks show decreasing trends in all three countries and these trends are consistent with the GOCI PM_{2.5} for both areal and population-weighted means, demonstrating that the trends reported by the PM_{2.5} networks are representative of the countries. However, the PM_{2.5} networks in eastern China and South Korea underestimate the population-weighted means. Trends in South Korea and eastern China become flat between 2018 and 2019 (with a slight population-weighted increase in South Korea). This could possibly reflect interannual meteorological variability [Zhai *et al.*, 2019; Koo *et al.*, 2020], but also an increase in oxidants producing secondary aerosol [Huang *et al.*, 2021]. **Figure S2** shows maps of annual GOCI PM_{2.5} across the entire study domain.

375

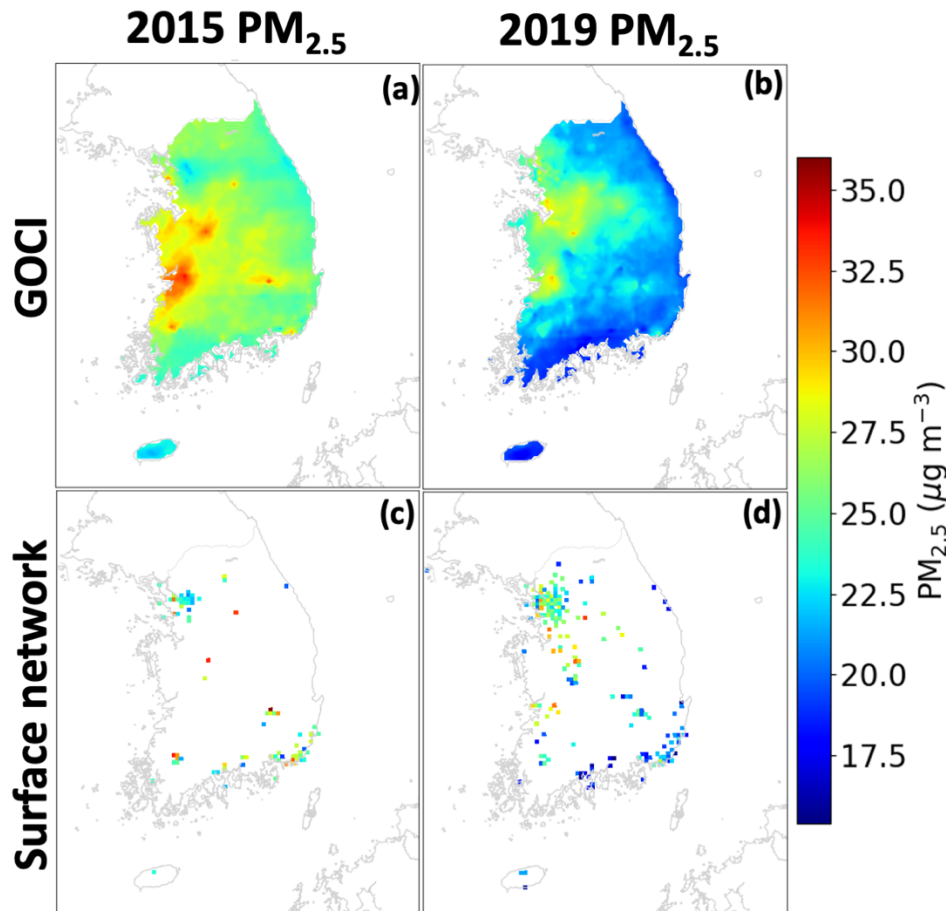


380

Figure 5: Trends in annual mean PM_{2.5} concentrations for eastern China, South Korea, and Japan. Trends determined from the national surface PM_{2.5} networks (dashed black line) averaged over 6x6 km² grid cells, requiring at least 80% of data for all years plotted, are compared to GOCI PM_{2.5} trends inferred by the random forest (RF) algorithm with continuous temporal and spatial coverage on the 6x6 km² grid and weighted either by area (solid colored line) or by population (dashed colored line). Here we use an RF trained on all the data. Gridded

population data are from CIESIN [2018]. The national PM_{2.5} networks include 413 continuously observed grid cells in eastern China, 74 in South Korea, and 307 in Japan. Trends are initialized at the onset of the surface network for complete years of data; due to the unavailability of the early months of the year, 2011 is discarded for Japan and 2014 for eastern China.

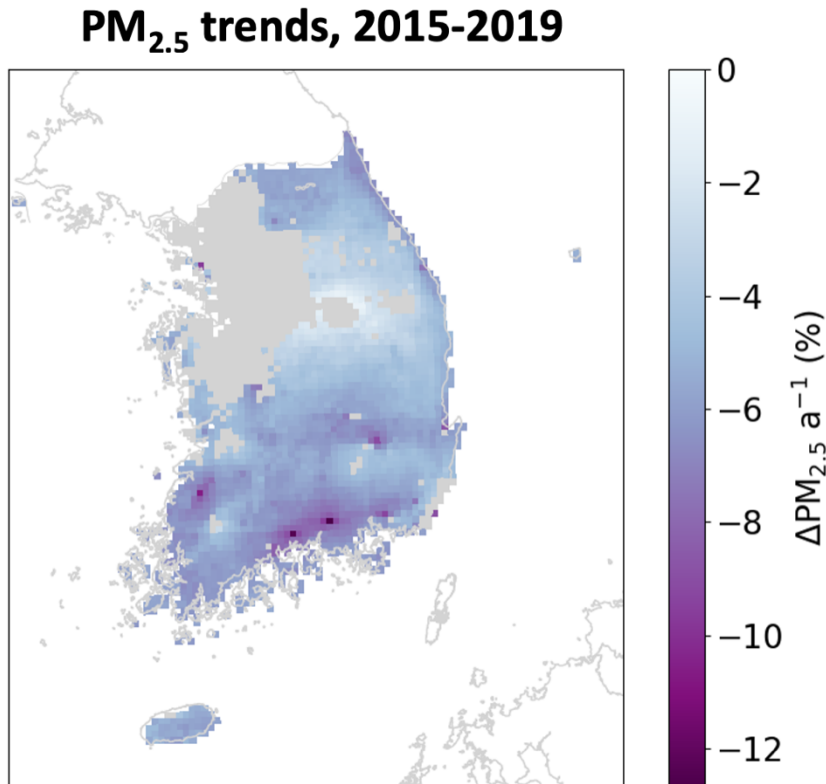
385 **Figure 6** shows the changes in annual mean PM_{2.5} concentrations over South Korea between
2015 and 2019 as observed from the national network and as inferred from GOCI. We focus on South
Korea here because it demonstrates how GOCI PM_{2.5} adds considerable information to a region that
already has relatively good network coverage, including detection of PM_{2.5} hotspots missing from the
network such as the Iksan region on the west coast in 2015 that was subsequently added to the network
390 by 2019. **Figures S3** and **S4** show analogous maps for China and Japan, respectively.



395 Figure 6: Annual mean PM_{2.5} concentrations in South Korea in 2015 and 2019. GOCI PM_{2.5} (top) inferred from an RF trained on all available data are compared to AirKorea network observations (bottom). Network observations are shown only if at least 80% of the year was observed.

Figure 7 depicts the relative 2015-2019 trends of PM_{2.5} concentrations in South Korea derived from a linear regression applied to the annual GOCI PM_{2.5} in each 6x6 km² grid cell. Such a spatially resolved trend analysis is uniquely enabled by the GOCI coverage. We find decreases across the country except in the Seoul Metropolitan area which mostly shows no significant trend except for a few

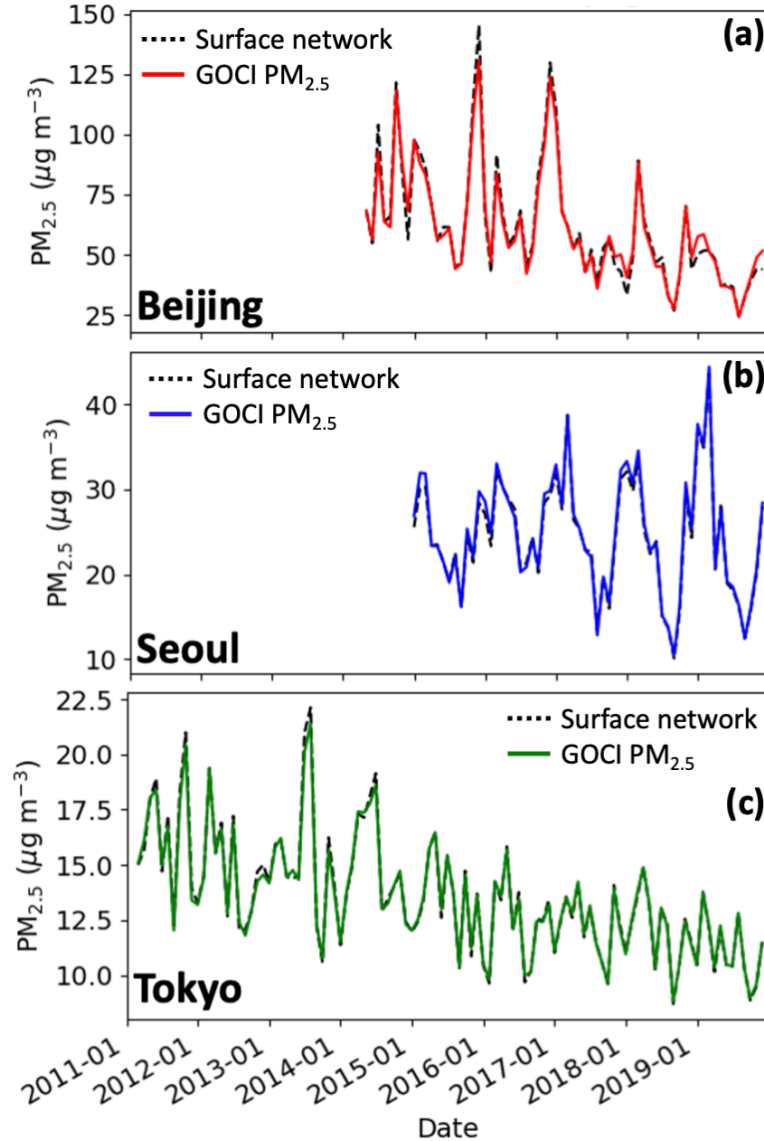
400 pixels in Incheon. These results are consistent with the spatial patterns calculated from AirKorea data by *Yeo and Kim* [2019], who found 2015-2018 decreases in Incheon but not Seoul or the surrounding Gyeonggi province. Despite the insignificant changes in Seoul, substantial $PM_{2.5}$ decreases are found over other large urban areas including Busan, Ulsan, Daegu, and Gwangju. The three rapidly decreasing spots on the southern coast are Gwangyang, Sacheon, and Changwon, which house industrial
405 complexes related to the South Korean shipbuilding industry that has recently declined [*Jung-a* 2016]. **Figure S5** shows absolute 2015-2019 trends of GOCI $PM_{2.5}$ concentrations across the entire study domain, and demonstrates that the North China Plain has the largest overall $PM_{2.5}$ reductions.



410 Figure 7: 2015-2019 trends per year in $PM_{2.5}$ concentrations across South Korea. The trends are obtained by ordinary linear regression of the annual mean GOCI $PM_{2.5}$ in each $6 \times 6 \text{ km}^2$ grid cell with significant regression slopes ($p < 0.05$), where the RF is trained on all the available data. Grid cells with insignificant trends are plotted in gray.

AOD and $PM_{2.5}$ in East Asia tend to have opposite seasonalities driven by boundary layer depth and RH [*Zhai et al.*, 2021]. **Figure 8** compares GOCI and surface network monthly mean $PM_{2.5}$ in the
415 Beijing, Seoul, and Tokyo metropolitan areas, with predictions coming from withheld data in the 10-fold crossvalidation. Correspondence between GOCI and network $PM_{2.5}$ may be tighter than the nationwide annual means plotted in **Figure 5** because these urban areas are well-observed. We see that the RF algorithm fully captures the observed seasonality in $PM_{2.5}$, although some observed monthly spikes are underestimated. The Figure illustrates the lack of trend in the Seoul Metropolitan Area over

420 2015-2019 but also shows that winter and summer $PM_{2.5}$ in the region have opposite and roughly equal trends, with winter growing more polluted while summers become cleaner.



425 Figure 8: Monthly $PM_{2.5}$ concentrations in the Beijing Seoul and Tokyo metropolitan areas. GOCI $PM_{2.5}$ inferred from the RF algorithm for totally withheld sites in the crossvalidation are compared to network observations. Beijing is defined by the namesake province boundary, Seoul by the Seoul and Incheon boundaries, and Tokyo as Ibaraki, Saitama, Chiba, Tokyo, Kanagawa, and Yamanashi prefectures.

3.3 Urban-scale pollution events

430 We examine here the ability of GOCI $PM_{2.5}$ to capture the spatial and temporal variability of $PM_{2.5}$ pollution events on urban scales. **Figure 9** shows a map of GOCI $PM_{2.5}$ — produced by a RF trained on all the data, with surface network $PM_{2.5}$ overlaid — across the Seoul metropolitan area on

435 May 24-29, 2016 corresponding to a severe pollution event sampled during the KORUS-AQ field campaign [Crawford *et. al.*, 2021]. The dense PM_{2.5} network for Seoul shows large variability at the sub 6x6 km² scale that GOCI does not resolve. However, GOCI PM_{2.5} captures most of the variability in the network data aggregated on the 6x6 km² grid (R² = 0.74). It also captures successfully the day-to-day variability during the event.

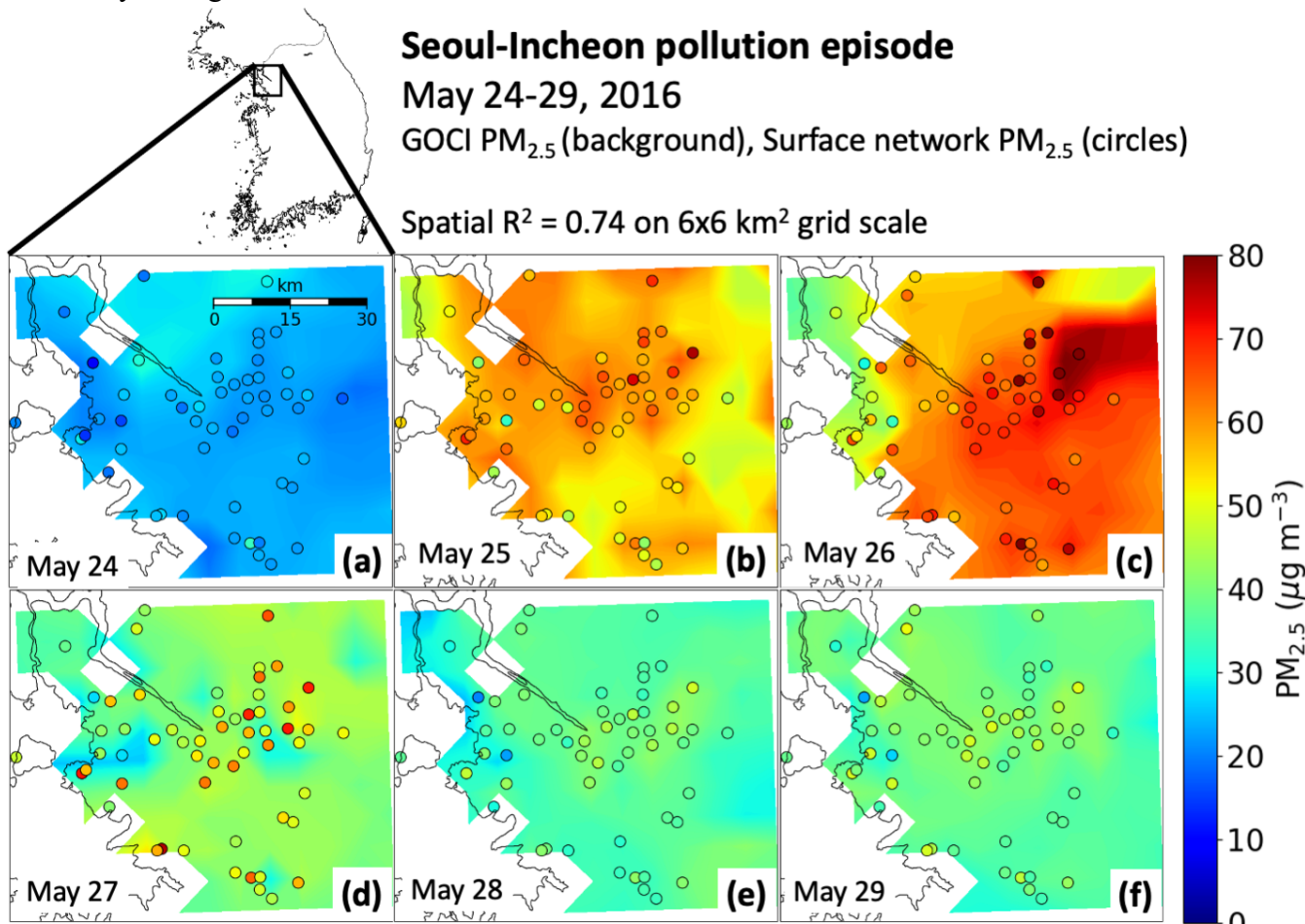


Figure 9: 24-h PM_{2.5} concentrations during a pollution event in Seoul-Incheon (May 24-29, 2016). GOCI PM_{2.5} inferred from the RF algorithm (background, on 6x6 km² grid scale) trained on all available data is compared to observations from the AirKorea surface network (circles).

440 **Figure 10** shows an additional test of the RF algorithm with one of the most severe pollution events in the record, the December 16-21, 2016 Beijing winter haze episode. 24-h PM_{2.5} concentrations exceeded 400 µg m⁻³ at some of the network sites. While there is a tight correspondence between the GOCI and surface network 24-h PM_{2.5} for Beijing grid cells (R² range: 0.74-0.99), the network observations are on average 20 µg m⁻³ higher than the GOCI PM_{2.5}. The difference is most pronounced at the December 21 concentration peak which has mean observed value 396 µg m⁻³ to the predicted 348 µg m⁻³. This reflects the RF smoothing and AOD underestimate for the high tail of the distribution as previously illustrated in **Figure 4**. It nevertheless illustrates the ability of GOCI combined with our

445

gap-filling method to capture severe winter haze episodes that are particularly challenging to observe from space.

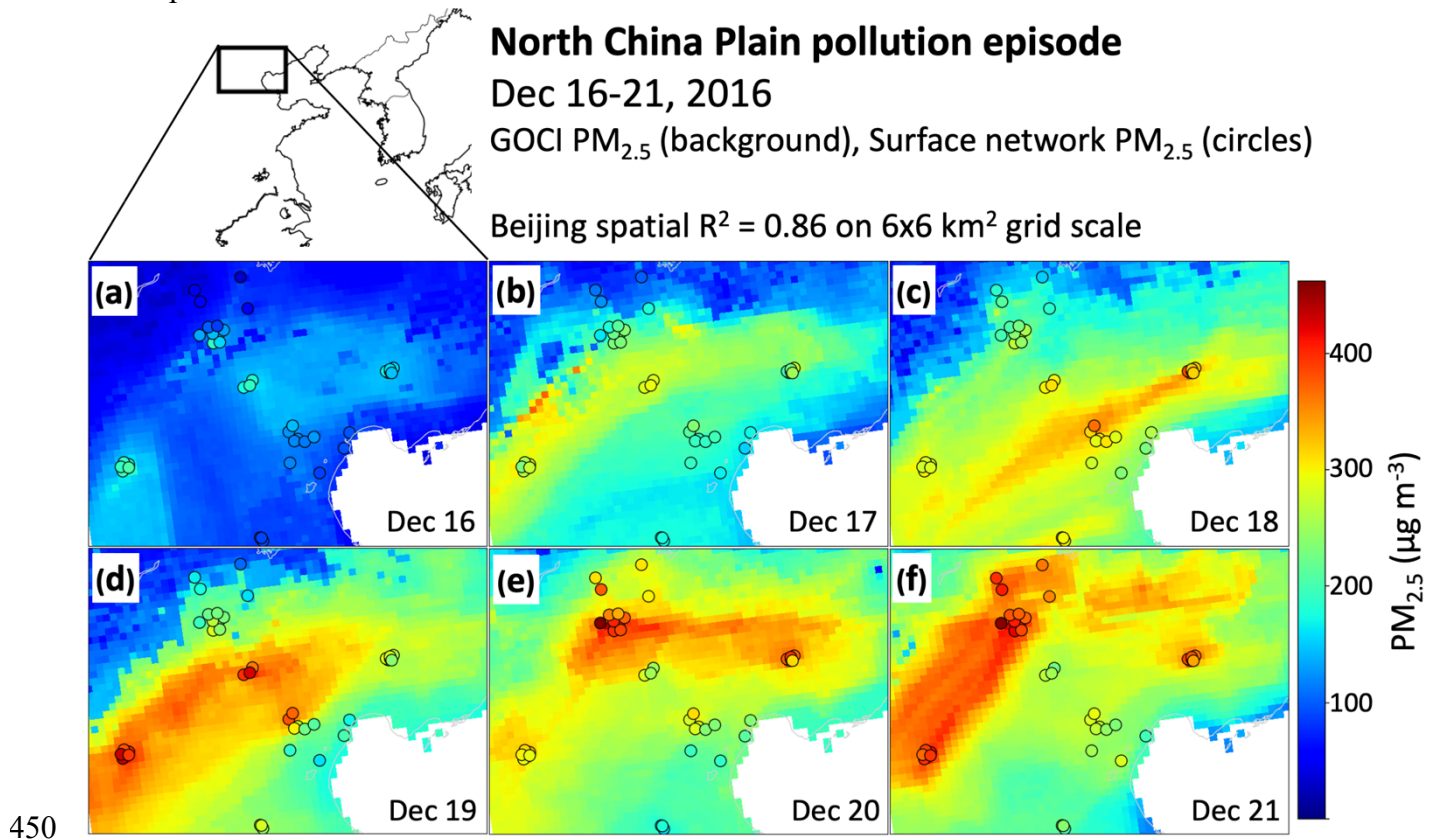


Figure 10: Same as Figure 9 but for a pollution event in Beijing on December 16-21, 2016.

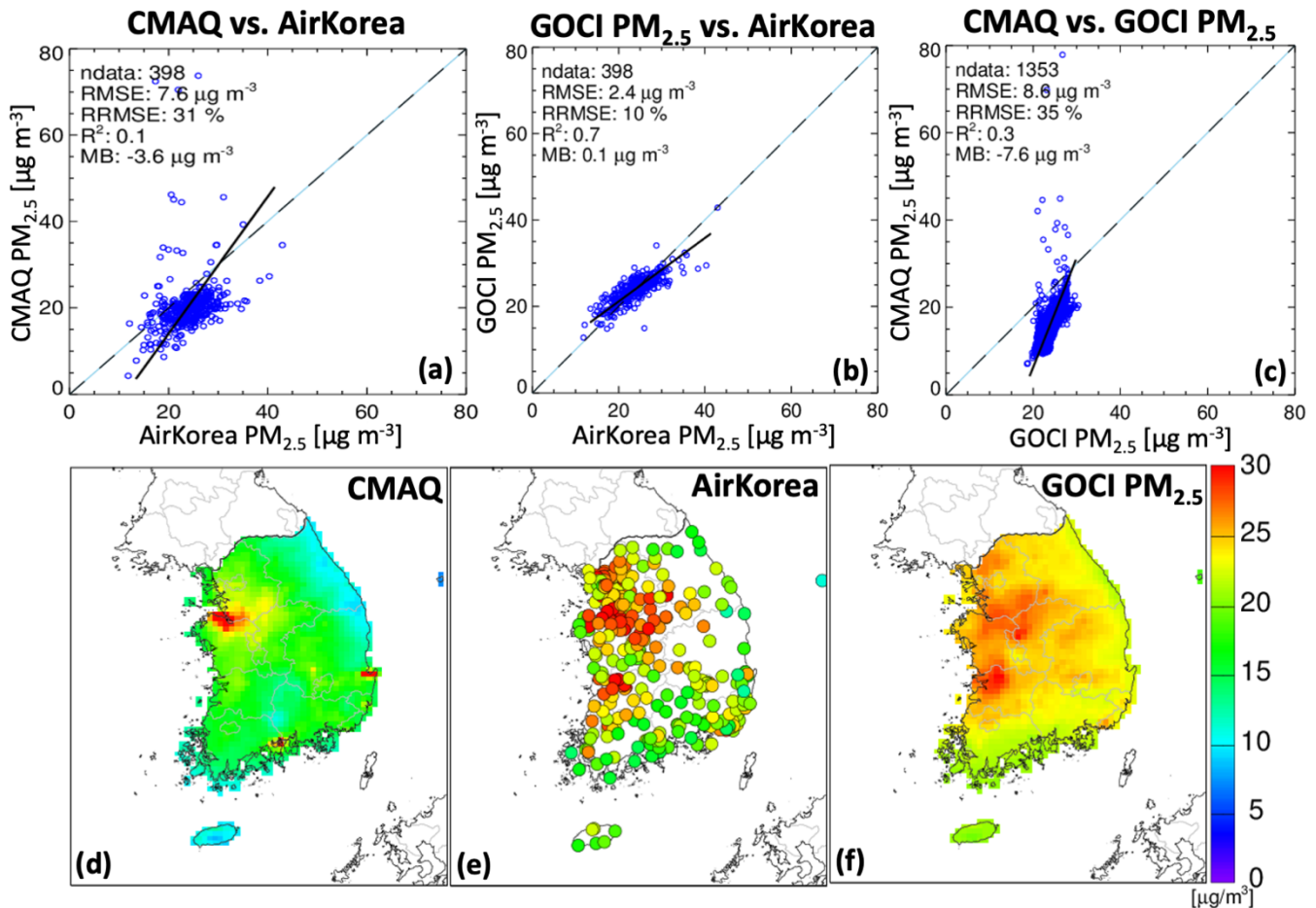
3.4 Regional air quality model evaluation

Regional air quality model predictions of PM_{2.5} are typically evaluated with observations from surface network sites, but the spatially continuous GOCI PM_{2.5} fields offer more extensive coverage and hence broader opportunity for model evaluation. We demonstrate this capability here with Community Multiscale Air Quality Modeling System (CMAQ version 4.7.1) simulations for the Korean peninsula including both South and North Korea at 9-km resolution [Bae *et al.*, 2018; Bae *et al.*, 2021]. There are no surface PM_{2.5} data in North Korea to train the RF so we use the South Korea categorical variable to generate the GOCI PM_{2.5} fields there.

460 The simulation for South Korea was conducted for 2015-2019 using emissions from the Clean Air Policy Support System (CAPSS) 2016 [Choi *et al.*, 2020] for South Korea and KORUSv5 [Woo *et al.*, n.d] for outside South Korea. The simulation for North Korea was conducted for 2016 using emissions from the Comprehensive Regional Emissions Inventory for Atmospheric Transport Experiment (CREATE) 2015 [Woo *et al.*, 2020] and CAPSS 2013. Natural aerosols including sea salt

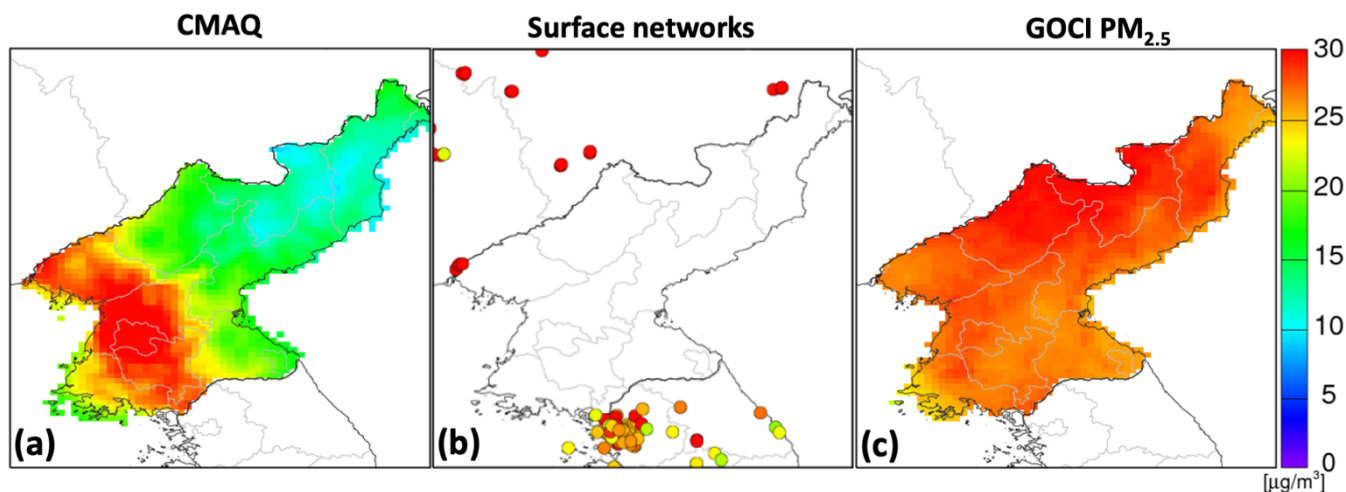
465 and mineral dust are included. To prepare the boundary conditions, a coarse domain at 27-km horizontal
grid resolution covering Northeast Asia was used.

Figure 11 illustrates the increased capability for model evaluation in South Korea enabled by
the GOCI PM_{2.5} fields. The bottom row shows the mean 2015-2019 PM_{2.5} concentrations in CMAQ
compared to the AirKorea network and to GOCI PM_{2.5}, and the top row shows comparison scatterplots.
470 The top left panel compares the CMAQ simulation to 2015-2019 mean PM_{2.5} observations from the 398
AirKorea network sites. The top middle panel compares the GOCI PM_{2.5} to the same AirKorea network
data, showing excellent agreement. The GOCI PM_{2.5} fields provide 1353 points for South Korea on the
9x9 km² CMAQ grid, and the top right panel shows the resulting increase in capability for evaluation of
the CMAQ simulation. It shows in particular that CMAQ underestimates PM_{2.5} in coastal environments,
475 possibly because of unaccounted ship emissions.



480 Figure 11: Mean PM_{2.5} concentrations in South Korea in 2015-2019 as simulated by CMAQ, measured at the AirKorea sites, and inferred
from GOCI. The top panels show scatterplots comparing the CMAQ and GOCI PM_{2.5} fields to the Air Korea measurements (398 sites), and
CMAQ to GOCI PM_{2.5} on the 9x9 km² CMAQ grid (1353 grid cells to compare). The bottom panels show maps of the mean 2015-2019
concentrations.

Figure 12 evaluates the CMAQ simulation with the GOCI PM_{2.5} fields over North Korea. Unlike in South Korea, there are no observation sites in North Korea and GOCI PM_{2.5} offers the only opportunity for local evaluation. CMAQ and GOCI PM_{2.5} show dramatically different patterns. The highest PM_{2.5} in CMAQ is in the Pyongyang capital region, while GOCI shows highest values in the north-central region. The lack of reliable emission inventories for North Korea makes it difficult to arbitrate this difference. The RF is not trained for North Korea, which might lead to positive biases because the AOD/PM_{2.5} ratio modeled in the *Zhai et al.* [2021] GEOS-Chem simulation is higher over North Korea outside the mountainous east (range: 0.010-0.013 m³ μg⁻¹) than over South Korea (0.008-0.010 m³ μg⁻¹). However, the difference could also be explained by missing emissions in the inventory. Further evaluation could be done with border sites in South Korea and northeastern China. China MEE sites along the border are consistent with high PM_{2.5} in north-central North Korea.



495 Figure 12: Mean PM_{2.5} concentrations in North Korea in 2016 as simulated by CMAQ and as represented by the GOCI PM_{2.5} product assuming South Korea as categorical variable. The middle panel shows surface PM_{2.5} concentrations from the AirKorea and China MEE networks.

4 Conclusions

We used 2011-2019 geostationary aerosol optical depth (AOD) observations from the GOCI satellite instrument, in combination with a random forest (RF) machine learning algorithm trained on air quality network data, to produce a continuous 24-h PM_{2.5} data set for eastern China, South Korea, and Japan at 6x6 km² resolution. The resulting gap-free GOCI PM_{2.5} product complements the air quality networks that cover only 1% of 6x6 km² grid cells in eastern China, 7% in South Korea, and 8% in Japan. It provides a general dataset for PM_{2.5} mapping to serve regional pollution analysis, air quality monitoring, and public health applications.

We trained the RF algorithm on gap-filled AODs from the GOCI instrument and a suite of twelve meteorological, geographical, and temporal predictor variables. Gap filling of AODs was done by a weighted combination of nearest-neighbor data and chemical transport model fields, with the weight serving as an additional predictor variable. The RF algorithm is successfully able to exploit

510 information encoded in AOD missingness to produce a continuous product. Testing of the RF algorithm
by prediction of withheld network sites shows single-value precisions in each country of 26-32% for 24-
h $PM_{2.5}$ and 12% for annual mean $PM_{2.5}$, with negligible mean bias. Accuracy statistics for $PM_{2.5}$
inferred on grid cells with no AOD retrieval (i.e., estimated using equation (1)) show similar accuracy
statistics as the entire population, indicating that the gap-filling procedure does not bias the results. The
515 algorithm has only moderate success at predicting NAAQS exceedance events because most of these
events are within the single-value precision, and also because of some smoothing of the extreme high
tail of the $PM_{2.5}$ frequency distribution.

We compared the continuous 24-h GOCI $PM_{2.5}$ fields to spatial and temporal patterns observed
at the national network sites. National trends of $PM_{2.5}$ inferred from GOCI and weighted by area or
520 population are consistent with those observed at network sites (2015-2019 in eastern China and South
Korea, 2011-2019 in Japan), confirming that the trends observed at these sites are representative.
However, the network sites in eastern China and South Korea underestimate population exposure. The
GOCI $PM_{2.5}$ fields over South Korea show $PM_{2.5}$ hotspots missing in the early AirKorea network (2015)
that are confirmed by subsequent addition of sites to the network (2019). The spatial distribution of
525 GOCI $PM_{2.5}$ trends in South Korea shows decreases everywhere except in the Seoul metropolitan area
where trends are flat. We show with time series in the capital cities (Beijing, Seoul, Tokyo) that the RF
successfully captures the seasonality of $PM_{2.5}$ even though AOD and $PM_{2.5}$ have different and often
opposite seasonalities.

We examined the ability of the RF algorithm to map air quality on urban scales by analysis of
530 two multi-day pollution episodes in Seoul and Beijing. The algorithm captures the day-to-day temporal
variability observed by the surface networks as well the spatial variability on the 6x6 km² scale. The
highest $PM_{2.5}$ concentrations are underpredicted, which reflects the smoothing of the high tail of the
distribution.

The continuous spatial coverage of $PM_{2.5}$ provided by the GOCI fields enables improved
535 evaluation of the air quality models used in support of emission control policies. Comparison to a
CMAQ simulation for South Korea in 2015-2019 reveals a large model underestimate in coastal
environments undersampled by the AirKorea network. Comparison to a CMAQ simulation for North
Korea in 2016, where the RF provides the only $PM_{2.5}$ data for model evaluation, shows drastically
different patterns with the RF featuring high $PM_{2.5}$ throughout North Korea. The RF results in North
540 Korea could be affected by errors due to lack of training data but they appear consistent with the $PM_{2.5}$
network observations at Chinese border sites.

More work could be done to improve our GOCI $PM_{2.5}$ product. We find in our current RF
algorithm, consistent with *Hu et al.* [2017], that the addition of certain predictor variables such as
population decreases performance. This motivated our practice of excluding spatially varying but
545 temporally constant fields such as elevation and emissions. However, these variables have been found
to be useful in other inferences of $PM_{2.5}$ from AOD data [*Kloog et al.*, 2012; *Di et al.*, 2019], so further
investigation is needed on how to accommodate them in our modeling framework. A higher resolution
meteorological reanalysis such as ERA5-Land [*Muñoz-Sabater et al.*, 2021] could be used for the
meteorological predictor variables and enable the inclusion of additional variables such as precipitation.
550 Additional remote sensing products such as NDVI could also be useful. More work needs to be done to
address our underestimate of the high tail of the $PM_{2.5}$ distribution, i.e., extreme pollution events. Such

an underestimate is common in RF applications [Zhang and Lu, 2012] but could be addressed by leveraging specialized statistical tools like extreme value theory. Additional training methods could be used to improve the ability of the RF to predict NAAQS exceedances, such as data sampling adjustments. Moreover, it is possible that skill in modeling NAAQS exceedance could be improved by leveraging data that better captures diurnal variations of PM_{2.5}, as high concentrations tend to occur at night. The unique geostationary capability of GOCI to generate hourly AOD data could be used to produce an hourly PM_{2.5} product. A new GOCI AOD product with 2x2 km² resolution is expected to become available in the near future and will provide motivation to explore these improvements in a new version of our RF algorithm.

Data availability 24-h 6x6 km² resolution daily GOCI PM_{2.5} are made freely available on DataVerse at <https://doi.org/10.7910/DVN/0L3IP7>.

Author Contributions DP and DJJ designed the study. DP developed the RF and performed analysis. SZ, MB and SK ran and analyzed chemical transport model data. SL aided in satellite data processing. JK, HL and JHK provided scientific interpretation and discussion. All authors provided input on the paper for revision before submission.

Competing interests The authors declare that they have no conflict of interest.

Acknowledgements This work was funded by the Samsung PM_{2.5} Strategic Research Program and the Harvard-NUIST Joint Laboratory for Air Quality and Climate (JLAQC). GOCI data was provided by Korea Institute of Ocean Science and Technology (KIOST). DCP was funded by a US National Science Foundation Graduate Fellowship. We thank the two anonymous reviewers for their thoughtful feedback.

References

- Alduchov, O. A., & Eskridge, R. E. (1996). Improved Magnus Form Approximation of Saturation Vapor Pressure. *Journal of Applied Meteorology*, 35(4), 601–609. [https://doi.org/10.1175/1520-0450\(1996\)035<0601:IMFAOS>2.0.CO;2](https://doi.org/10.1175/1520-0450(1996)035<0601:IMFAOS>2.0.CO;2)
- Azuma, K., Kagi, N., Kim, H., & Hayashi, M. (2020). Impact of climate and ambient air pollution on the epidemic growth during COVID-19 outbreak in Japan. *Environmental Research*, 190, 110042. <https://doi.org/10.1016/j.envres.2020.110042>
- Bae, M., Kim, H. C., Kim, B.-U., and Kim, S.: PM_{2.5} Simulations for the Seoul Metropolitan Area: (V) Estimation of North Korean Emission Contribution, *J. Korean Soc. Atmos. Environ.*, 34, 294–305, <https://doi.org/10.5572/KOSAE.2018.34.2.294>, 2018.
- Bae, M., Kim, B.-U., Kim, H. C., Kim, J., and Kim, S.: Role of emissions and meteorology in the recent PM_{2.5} changes in China and South Korea from 2015 to 2018, *Environmental Pollution*, 270, 116233, <https://doi.org/10.1016/j.envpol.2020.116233>, 2021.
- Brasseur, G. P. and Jacob, D. J (2017). *Modeling of Atmospheric Chemistry*. Cambridge University Press.

- Breiman, L. (2001). Random Forests. *Machine Learning*, 45(1), 5–32.
<https://doi.org/10.1023/A:1010933404324>
- Brokamp, C., Jandarov, R., Hossain, M., & Ryan, P. (2018). Predicting Daily Urban Fine Particulate Matter Concentrations Using a Random Forest Model. *Environmental Science & Technology*, 52(7), 4173–4179. <https://doi.org/10.1021/acs.est.7b05381>
- 595 Burnett, R., et. al. (2018). Global estimates of mortality associated with long-term exposure to outdoor fine particulate matter. *Proceedings of the National Academy of Sciences*, 115(38), 9592–9597.
<https://doi.org/10.1073/pnas.1803222115>
- Center for International Earth Science Information Network – CIESIN – Columbia University. 2018. Gridded Population of the World, Version 4 (GPWv4): Population Density, Revision 11. Palisades, NY: NASA Socioeconomic Data and Applications Center (SEDAC).
<https://doi.org/10.7927/H49C6VHW>
- 600 Chen, J., Yin, J., Zang, L., Zhang, T., & Zhao, M. (2019). Stacking machine learning model for estimating hourly PM_{2.5} in China based on Himawari 8 aerosol optical depth data. *Science of The Total Environment*, 697, 134021. <https://doi.org/10.1016/j.scitotenv.2019.134021>
- 605 Chinese State Council (2013). Action Plan on Air Pollution Prevention and Control, available at: http://www.gov.cn/zwggk/2013-09/12/content_2486773.htm (last access: 12 April 2021).
- Choi, J.-K., Park, Y. J., Ahn, J. H., Lim, H.-S., Eom, J., & Ryu, J.-H. (2012). GOCI, the world’s first geostationary ocean color observation satellite, for the monitoring of temporal variability in coastal water turbidity. *Journal of Geophysical Research: Oceans*, 117(C9).
<https://doi.org/10.1029/2012JC008046>
- 610 Choi, M., Kim, J., Lee, J., Kim, M., Park, Y.-J., Jeong, U., Kim, W., Hong, H., Holben, B., Eck, T. F., Song, C. H., Lim, J.-H., & Song, C.-K. (2016). GOCI Yonsei Aerosol Retrieval (YAER) algorithm and validation during the DRAGON-NE Asia 2012 campaign. *Atmospheric Measurement Techniques*, 9(3), 1377–1398. <https://doi.org/10.5194/amt-9-1377-2016>
- 615 Choi, M., Kim, J., Lee, J., Kim, M., Park, Y.-J., Holben, B., Eck, T. F., Li, Z., & Song, C. H. (2018). GOCI Yonsei aerosol retrieval version 2 products: An improved algorithm and error analysis with uncertainty estimation from 5-year validation over East Asia. *Atmospheric Measurement Techniques*, 11(1), 385–408. <https://doi.org/10.5194/amt-11-385-2018>
- 620 Choi, M., Lim, H., Kim, J., Lee, S., Eck, T. F., Holben, B. N., Garay, M. J., Hyer, E. J., Saide, P. E., & Liu, H. (2019). Validation, comparison, and integration of GOCI, AHI, MODIS, MISR, and VIIRS aerosol optical depth over East Asia during the 2016 KORUS-AQ campaign. *Atmospheric Measurement Techniques*, 12(8), 4619–4641. <https://doi.org/10.5194/amt-12-4619-2019>
- 625 Choi, S., Kim, T., Lee, H., Kim, H., Han, J., Lee, K., Lim, E., Shin, S., Jin, H., Cho, E., Kim, Y., and Yoo, C.: Analysis of the National Air Pollutant Emission Inventory (CAPSS 2016) and the Major Cause of Change in Republic of Korea, 14, 24, 2020.
- 630 Crawford, J. H., Ahn, J.-Y., Al-Saadi, J., Chang, L., Emmons, L. K., Kim, J., Lee, G., Park, J.-H., Park, R. J., Woo, J. H., Song, C.-K., Hong, J.-H., Hong, Y.-D., Lefer, B. L., Lee, M., Lee, T., Kim, S., Min, K.-E., Yum, S. S., ... Kim, Y. P. (2021). The Korea–United States Air Quality (KORUS-AQ) field study. *Elementa: Science of the Anthropocene*, 9(1).
<https://doi.org/10.1525/elementa.2020.00163>

- Cusworth, D. H., Jacob, D. J., Sheng, J.-X., Benmergui, J., Turner, A. J., Brandman, J., White, L., & Randles, C. A. (2018). Detecting high-emitting methane sources in oil/gas fields using satellite observations. *Atmospheric Chemistry and Physics*, 18(23), 16885–16896. <https://doi.org/10.5194/acp-18-16885-2018>
- 635
- Di, Q., Amini, H., Shi, L., Kloog, I., Silvern, R., Kelly, J., Sabath, M. B., Choirat, C., Koutrakis, P., Lyapustin, A., Wang, Y., Mickley, L. J., & Schwartz, J. (2019). An ensemble-based model of PM_{2.5} concentration across the contiguous United States with high spatiotemporal resolution. *Environment International*, 130, 104909. <https://doi.org/10.1016/j.envint.2019.104909>
- 640
- Dominici, F., Peng, R. D., Bell, M. L., Pham, L., McDermott, A., Zeger, S. L., & Samet, J. M. (2006). Fine particulate air pollution and hospital admission for cardiovascular and respiratory diseases. *JAMA*, 295(10), 1127–1134. <https://doi.org/10.1001/jama.295.10.1127>
- Gaspari, G., & Cohn, S. E. (1999). Construction of correlation functions in two and three dimensions. *Quarterly Journal of the Royal Meteorological Society*, 125(554), 723–757. <https://doi.org/10.1002/qj.49712555417>
- 645
- Geng, G., Zhang, Q., Martin, R. V., van Donkelaar, A., Huo, H., Che, H., Lin, J., & He, K. (2015). Estimating long-term PM_{2.5} concentrations in China using satellite-based aerosol optical depth and a chemical transport model. *Remote Sensing of Environment*, 166, 262–270. <https://doi.org/10.1016/j.rse.2015.05.016>
- 650
- Geng, G., Meng, X., He, K., & Liu, Y. (2020). Random forest models for PM_{2.5} speciation concentrations using MISR fractional AODs. *Environmental Research Letters*, 15(3), 034056. <https://doi.org/10.1088/1748-9326/ab76df>
- Geurts, P., Ernst, D., & Wehenkel, L. (2006). Extremely randomized trees. *Machine Learning*, 63(1), 3–42. <https://doi.org/10.1007/s10994-006-6226-1>
- 655
- Gräler, B., Pebesma, E., & Heuvelink, G. (2016). Spatio-Temporal Interpolation using gstat. *The R Journal*, 8(1), 204–218.
- Gupta, P., & Christopher, S. A. (2009). Particulate matter air quality assessment using integrated surface, satellite, and meteorological products: Multiple regression approach. *Journal of Geophysical Research: Atmospheres*, 114(D14). <https://doi.org/10.1029/2008JD011496>
- 660
- Guo, B., Zhang, D., Pei, L., Su, Y., Wang, X., Bian, Y., Zhang, D., Yao, W., Zhou, Z., & Guo, L. (2021). Estimating PM_{2.5} concentrations via random forest method using satellite, auxiliary, and ground-level station dataset at multiple temporal scales across China in 2017. *Science of The Total Environment*, 778, 146288. <https://doi.org/10.1016/j.scitotenv.2021.146288>
- 665
- Hammer, M. S., van Donkelaar, A., Li, C., Lyapustin, A., Sayer, A. M., Hsu, N. C., Levy, R. C., Garay, M. J., Kalashnikova, O. V., Kahn, R. A., Brauer, M., Apte, J. S., Henze, D. K., Zhang, L., Zhang, Q., Ford, B., Pierce, J. R., & Martin, R. V. (2020). Global Estimates and Long-Term Trends of Fine Particulate Matter Concentrations (1998–2018). *Environmental Science & Technology*, 54(13), 7879–7890. <https://doi.org/10.1021/acs.est.0c01764>
- 670
- Hastie, T., Tibshirani, R., & Friedman, J. (2009). Random Forests. In *The Elements of Statistical Learning: Data Mining, Inference, and Prediction* (pp. 587–604). Springer. https://doi.org/10.1007/978-0-387-84858-7_15
- Hersbach, H., Bell, B., Berrisford, P., Hirahara, S., Horányi, A., Muñoz-Sabater, J., Nicolas, J., Peubey, C., Radu, R., Schepers, D., Simmons, A., Soci, C., Abdalla, S., Abellan, X., Balsamo, G.,

- 675 Bechtold, P., Biavati, G., Bidlot, J., Bonavita, M., ... Thépaut, J.-N. (2020). The ERA5 global reanalysis. *Quarterly Journal of the Royal Meteorological Society*, 146(730), 1999–2049. <https://doi.org/10.1002/qj.3803>
- Hu, H., Hu, Z., Zhong, K., Xu, J., Zhang, F., Zhao, Y., & Wu, P. (2019). Satellite-based high-resolution mapping of ground-level PM_{2.5} concentrations over East China using a spatiotemporal regression kriging model. *Science of The Total Environment*, 672, 479–490. <https://doi.org/10.1016/j.scitotenv.2019.03.480>
- 680 Hu, X., Belle, J. H., Meng, X., Wildani, A., Waller, L. A., Strickland, M. J., & Liu, Y. (2017). Estimating PM_{2.5} Concentrations in the Conterminous United States Using the Random Forest Approach. *Environmental Science & Technology*, 51(12), 6936–6944. <https://doi.org/10.1021/acs.est.7b01210>
- 685 Huang, K., Xiao, Q., Meng, X., Geng, G., Wang, Y., Lyapustin, A., Gu, D., & Liu, Y. (2018). Predicting monthly high-resolution PM_{2.5} concentrations with random forest model in the North China Plain. *Environmental Pollution*, 242, 675–683. <https://doi.org/10.1016/j.envpol.2018.07.016>
- 690 Huang, X., Ding, A., Gao, J., Zheng, B., Zhou, D., Qi, X., Tang, R., Wang, J., Ren, C., Nie, W., Chi, X., Xu, Z., Chen, L., Li, Y., Che, F., Pang, N., Wang, H., Tong, D., Qin, W., ... He, K. (2021). Enhanced secondary pollution offset reduction of primary emissions during COVID-19 lockdown in China. *National Science Review*, 8(2). <https://doi.org/10.1093/nsr/nwaa137>
- Jung-a, Song (2016). South Korean shipbuilders engulfed in crisis. *Financial Times*. <https://www.ft.com/content/d74127ac-3140-11e6-8825-ef265530038e>
- 695 Kianian, B., Liu, Y., & Chang, H. H. (2021). Imputing Satellite-Derived Aerosol Optical Depth Using a Multi-Resolution Spatial Model and Random Forest for PM_{2.5} Prediction. *Remote Sensing*, 13(1), 126. <https://doi.org/10.3390/rs13010126>
- Kiourmourtzoglou Marianthi-Anna, Schwartz Joel D., Weisskopf Marc G., Melly Steven J., Wang Yun, Dominici Francesca, & Zanobetti Antonella. (2016). Long-term PM_{2.5} Exposure and Neurological Hospital Admissions in the Northeastern United States. *Environmental Health Perspectives*, 124(1), 23–29. <https://doi.org/10.1289/ehp.1408973>
- 700 Koo, J.-H., Kim, J., Lee, Y. G., Park, S. S., Lee, S., Chong, H., Cho, Y., Kim, J., Choi, K., & Lee, T. (2020). The implication of the air quality pattern in South Korea after the COVID-19 outbreak. *Scientific Reports*, 10(1), 22462. <https://doi.org/10.1038/s41598-020-80429-4>
- 705 Kloog, I., Nordio, F., Coull, B. A., & Schwartz, J. (2012). Incorporating Local Land Use Regression And Satellite Aerosol Optical Depth In A Hybrid Model Of Spatio-Temporal PM_{2.5} Exposures In The Mid-Atlantic States. *Environmental Science & Technology*, 46(21), 11913–11921. <https://doi.org/10.1021/es302673e>
- 710 Kloog, I., Chudnovsky, A. A., Just, A. C., Nordio, F., Koutrakis, P., Coull, B. A., Lyapustin, A., Wang, Y., & Schwartz, J. (2014). A new hybrid spatio-temporal model for estimating daily multi-year PM_{2.5} concentrations across northeastern USA using high resolution aerosol optical depth data. *Atmospheric Environment*, 95, 581–590. <https://doi.org/10.1016/j.atmosenv.2014.07.014>
- 715 Li, T., Shen, H., Yuan, Q., Zhang, X., & Zhang, L. (2017). Estimating Ground-Level PM_{2.5} by Fusing Satellite and Station Observations: A Geo-Intelligent Deep Learning Approach. *Geophysical Research Letters*, 44(23), 11,985-11,993. <https://doi.org/10.1002/2017GL075710>

- Lim, H., Choi, M., Kim, J., Kasai, Y., & Chan, P. W. (2018). AHI/Himawari-8 Yonsei Aerosol Retrieval (YAER): Algorithm, Validation and Merged Products. *Remote Sensing*, 10(5), 699. <https://doi.org/10.3390/rs10050699>
- 720 Lim, H., Go, S., Kim, J., Choi, M., Lee, S., Song, C.-K., & Kasai, Y. (2021). Integration of GOCI and AHI Yonsei aerosol optical depth products during the 2016 KORUS-AQ and 2018 EMERG campaigns. *Atmospheric Measurement Techniques*, 14(6), 4575–4592. <https://doi.org/10.5194/amt-14-4575-2021>
- 725 Liu, Y., Park, R. J., Jacob, D. J., Li, Q., Kilaru, V., & Sarnat, J. A. (2004). Mapping annual mean ground-level PM_{2.5} concentrations using Multiangle Imaging Spectroradiometer aerosol optical thickness over the contiguous United States. *Journal of Geophysical Research: Atmospheres*, 109(D22). <https://doi.org/10.1029/2004JD005025>
- 730 Liu Yang, Paciorek Christopher J., & Koutrakis Petros. (2009). Estimating Regional Spatial and Temporal Variability of PM_{2.5} Concentrations Using Satellite Data, Meteorology, and Land Use Information. *Environmental Health Perspectives*, 117(6), 886–892. <https://doi.org/10.1289/ehp.0800123>
- Lyapustin, A., Wang, Y., Korkin, S., & Huang, D. (2018). MODIS Collection 6 MAIAC algorithm. *Atmospheric Measurement Techniques*, 11(10), 5741–5765. <https://doi.org/10.5194/amt-11-5741-2018>
- 735 Muñoz-Sabater, J., Dutra, E., Agustí-Panareda, A., Albergel, C., Arduini, G., Balsamo, G., Boussetta, S., Choulga, M., Harrigan, S., Hersbach, H., Martens, B., Miralles, D. G., Piles, M., Rodríguez-Fernández, N. J., Zsoter, E., Buontempo, C., & Thépaut, J.-N. (2021). ERA5-Land: A state-of-the-art global reanalysis dataset for land applications. *Earth System Science Data*, 13(9), 4349–4383. <https://doi.org/10.5194/essd-13-4349-2021>
- 740 Park, S., Shin, M., Im, J., Song, C.-K., Choi, M., Kim, J., Lee, S., Park, R., Kim, J., Lee, D.-W., and Kim, S.-K. (2019). Estimation of ground-level particulate matter concentrations through the synergistic use of satellite observations and process-based models over South Korea, *Atmos. Chem. Phys.*, 19, 1097–1113, <https://doi.org/10.5194/acp-19-1097-2019>.
- 745 Pedregosa, F., Varoquaux, G., Gramfort, A., Michel, V., Thirion, B., Grisel, O., Blondel, M., Prettenhofer, P., Weiss, R., Dubourg, V., Vanderplas, J., Passos, A., Cournapeau, D., Brucher, M., Perrot, M., & Duchesnay, É. (2011). Scikit-learn: Machine Learning in Python. *Journal of Machine Learning Research*, 12(85), 2825–2830.
- Phillips, Tom. Beijing smog: Pollution red alert declared in China capital and 21 other cities. (2016). *The Guardian*. <http://www.theguardian.com/world/2016/dec/17/beijing-smog-pollution-red-alert-declared-in-china-capital-and-21-other-cities> (last access: 13 April 2021)
- 750 Poulidis, A. P., Takemi, T., Shimizu, A., Iguchi, M., & Jenkins, S. F. (2018). Statistical analysis of dispersal and deposition patterns of volcanic emissions from Mt. Sakurajima, Japan. *Atmospheric Environment*, 179, 305–320. <https://doi.org/10.1016/j.atmosenv.2018.02.021>
- 755 Remer, L. A., Kaufman, Y. J., Tanré, D., Mattoo, S., Chu, D. A., Martins, J. V., Li, R.-R., Ichoku, C., Levy, R. C., Kleidman, R. G., Eck, T. F., Vermote, E., & Holben, B. N. (2005). The MODIS Aerosol Algorithm, Products, and Validation. *Journal of the Atmospheric Sciences*, 62(4), 947–973. <https://doi.org/10.1175/JAS3385.1>

- 760 Remer, L. A., Mattoo, S., Levy, R. C., Heidinger, A., Pierce, R. B., & Chin, M. (2012). Retrieving aerosol in a cloudy environment: Aerosol product availability as a function of spatial resolution. *Atmospheric Measurement Techniques*, 5(7), 1823–1840. <https://doi.org/10.5194/amt-5-1823-2012>
- 765 Remer, L. A., Mattoo, S., Levy, R. C., & Munchak, L. A. (2013). MODIS 3 km aerosol product: Algorithm and global perspective. *Atmospheric Measurement Techniques*, 6(7), 1829–1844. <https://doi.org/10.5194/amt-6-1829-2013>
- 770 She, Q., Choi, M., Belle, J. H., Xiao, Q., Bi, J., Huang, K., Meng, X., Geng, G., Kim, J., He, K., Liu, M., & Liu, Y. (2020). Satellite-based estimation of hourly PM_{2.5} levels during heavy winter pollution episodes in the Yangtze River Delta, China. *Chemosphere*, 239, 124678. <https://doi.org/10.1016/j.chemosphere.2019.124678>
- 775 Shepard, D. (1968). A two-dimensional interpolation function for irregularly-spaced data. *Proceedings of the 1968 23rd ACM National Conference*, 517–524. <https://doi.org/10.1145/800186.810616>
- 780 Stafoggia, M., Bellander, T., Bucci, S., Davoli, M., de Hoogh, K., de' Donato, F., Gariazzo, C., Lyapustin, A., Michelozzi, P., Renzi, M., Scortichini, M., Shtein, A., Viegi, G., Kloog, I., & Schwartz, J. (2019). Estimation of daily PM₁₀ and PM_{2.5} concentrations in Italy, 2013–2015, using a spatiotemporal land-use random-forest model. *Environment International*, 124, 170–179. <https://doi.org/10.1016/j.envint.2019.01.016>
- van Donkelaar, A. van, Martin, R. V., & Park, R. J. (2006). Estimating ground-level PM_{2.5} using aerosol optical depth determined from satellite remote sensing. *Journal of Geophysical Research: Atmospheres*, 111(D21). <https://doi.org/10.1029/2005JD006996>
- van Donkelaar Aaron, Martin Randall V., Brauer Michael, Kahn Ralph, Levy Robert, Verduzco Carolyn, & Villeneuve Paul J. (2010). Global Estimates of Ambient Fine Particulate Matter Concentrations from Satellite-Based Aerosol Optical Depth: Development and Application. *Environmental Health Perspectives*, 118(6), 847–855. <https://doi.org/10.1289/ehp.0901623>
- 785 van Donkelaar, A., et. al. (2016). Global Estimates of Fine Particulate Matter using a Combined Geophysical-Statistical Method with Information from Satellites, Models, and Monitors. *Environmental Science & Technology*, 50(7), 3762–3772. <https://doi.org/10.1021/acs.est.5b05833>
- 790 van Donkelaar, A., Martin, R. V., Li, C., & Burnett, R. T. (2019). Regional Estimates of Chemical Composition of Fine Particulate Matter Using a Combined Geoscience-Statistical Method with Information from Satellites, Models, and Monitors. *Environmental Science & Technology*, 53(5), 2595–2611. <https://doi.org/10.1021/acs.est.8b06392>
- Wang, J., and Christopher, S. A. (2003). Intercomparison between satellite-derived aerosol optical thickness and PM_{2.5} mass: Implications for air quality studies. *Geophysical Research Letters*, 30(21). <https://doi.org/10.1029/2003GL018174>
- 795 Wang, W., Mao, F., Du, L., Pan, Z., Gong, W., & Fang, S. (2017). Deriving Hourly PM_{2.5} Concentrations from Himawari-8 AODs over Beijing–Tianjin–Hebei in China. *Remote Sensing*, 9(8), 858. <https://doi.org/10.3390/rs9080858>
- Wei, Y., Wang, Y., Di, Q., Choirat, C., Wang, Y., Koutrakis, P., Zanobetti, A., Dominici, F., & Schwartz, J. D. (2019). Short term exposure to fine particulate matter and hospital admission

- risks and costs in the Medicare population: Time stratified, case crossover study. *BMJ*, 367, 16258. <https://doi.org/10.1136/bmj.l6258>
- 800 Woo, J.-H., Kim, Y., Kim, H.-K., Choi, K.-C., Eum, J.-H., Lee, J.-B., Lim, J.-H., Kim, J., and Seong, M.: Development of the CREATE Inventory in Support of Integrated Climate and Air Quality Modeling for Asia, *Sustainability*, 12, 7930, <https://doi.org/10.3390/su12197930>, 2020.
- 805 Woo, J.-H., Kim, Y., Kim, J., Park, M., Jang, Y., Kim, J., Bu, C., Lee, Y., Park, R., Oak, Y., Fried, A., Simpson, I., Emmons, L., Crawford, J. n.d. KORUS Emissions: A comprehensive Asian emissions information in support of the NASA/NIER KORUS-AQ mission. *Elementa: Science of the Anthropocene*, in press.
- 810 Xu, J.-W., Martin, R. V., van Donkelaar, A., Kim, J., Choi, M., Zhang, Q., Geng, G., Liu, Y., Ma, Z., Huang, L., Wang, Y., Chen, H., Che, H., Lin, P., & Lin, N. (2015). Estimating ground-level PM_{2.5} in eastern China using aerosol optical depth determined from the GOCI satellite instrument. *Atmospheric Chemistry and Physics*, 15(22), 13133–13144. <https://doi.org/10.5194/acp-15-13133-2015>
- 815 Xue, T., Zheng, Y., Tong, D., Zheng, B., Li, X., Zhu, T., & Zhang, Q. (2019). Spatiotemporal continuous estimates of PM_{2.5} concentrations in China, 2000–2016: A machine learning method with inputs from satellites, chemical transport model, and ground observations. *Environment International*, 123, 345–357. <https://doi.org/10.1016/j.envint.2018.11.075>
- 820 Yeo, M. and Kim, Y. (2019). Trends of the PM_{2.5} concentrations and high PM_{2.5} concentration cases by region in Korea. *Particle and Aerosol Research*, 15(2), 45-56. <http://dx.doi.org/10.11629/jpaar.2019.15.2.045> (in Korean).
- 825 Zang, L., Mao, F., Guo, J., Wang, W., Pan, Z., Shen, H., Zhu, B., & Wang, Z. (2019). Estimation of spatiotemporal PM_{1.0} distributions in China by combining PM_{2.5} observations with satellite aerosol optical depth. *Science of The Total Environment*, 658, 1256–1264. <https://doi.org/10.1016/j.scitotenv.2018.12.297>
- 830 Zhai, S., Jacob, D. J., Wang, X., Shen, L., Li, K., Zhang, Y., Gui, K., Zhao, T., & Liao, H. (2019). Fine particulate matter (PM_{2.5}) trends in China, 2013–2018: Separating contributions from anthropogenic emissions and meteorology. *Atmospheric Chemistry and Physics*, 19(16), 11031–11041. <https://doi.org/10.5194/acp-19-11031-2019>
- 835 Zhai, S., Jacob, D. J., Brewer, J. F., Li, K., Moch, J. M., Kim, J., Lee, S., Lim, H., Lee, H. C., Kuk, S. K., Park, R. J., Jeong, J. I., Wang, X., Liu, P., Luo, G., Yu, F., Meng, J., Martin, R. V., Travis, K. R., ... Liao, H. (2021). Interpretation of geostationary satellite aerosol optical depth (AOD) over East Asia in relation to fine particulate matter (PM_{2.5}): Insights from the KORUS-AQ aircraft campaign and seasonality. *Atmospheric Chemistry and Physics Discussions*, 1–23. <https://doi.org/10.5194/acp-2021-413>
- Zhang, G., & Lu, Y. (2012). Bias-corrected random forests in regression. *Journal of Applied Statistics*, 39(1), 151–160. <https://doi.org/10.1080/02664763.2011.578621>
- Zhuang, J., Dussin, R., Jüling, A., & Rasp, S. (2020). JiaweiZhuang/xESMF: v0.3.0 Adding ESMF.LocStream capabilities (Version v0.3.0). Zenodo. <https://doi.org/10.5281/ZENODO.1134365>